Redox Biology 51 (2022) 102280

Contents lists available at ScienceDirect

Redox Biology

journal homepage: www.elsevier.com/locate/redox

Theranostic F-SLOH mitigates Alzheimer's disease pathology involving TFEB and ameliorates cognitive functions in Alzheimer's disease models

Ashok Iyaswamy [a,b,1,****], Xueli Wang [c,1], Senthilkumar Krishnamoorthi [a,d,1], Venkatapathy Kaliamoorthy [a], Sravan G. Sreenivasmurthy [a,b], Siva Sundara Kumar Durairajan [e], Ju-Xian Song [a,f], Benjamin Chun-kit Tong [a,b], Zhou Zhu [a,b], Cheng-Fu Su [a,b], Jia Liu [a,b], King-Ho Cheung [a,b], Jia-Hong Lu [g], Jie-Qiong Tan [h], Hung Wing Li [i,***], Man Shing Wong [c,**], Min Li [a,b,*]

[a] Mr. & Mrs. Ko Chi-Ming Centre for Parkinson's Disease Research, School of Chinese Medicine, Hong Kong Baptist University, Hong Kong SAR, China
[b] Institute for Research and Continuing Education, Hong Kong Baptist University, Shenzhen, 518057, China
[c] Department of Chemistry, Hong Kong Baptist University, Hong Kong SAR, China
[d] Centre for Trans-disciplinary Research, Department of Pharmacology, Saveetha Dental College and Hospitals, Chennai, Tamil Nadu, India
[e] Division of Mycobiology and Neurodegenerative Disease Research, Department of Microbiology, School of Life Sciences, Central University of Tamil Nadu, Tiruvarur, India
[f] Medical College of Acupuncture-Moxibustion and Rehabilitation, Guangzhou University of Chinese Medicine, Guangzhou, China
[g] State Key Lab of Quality Research in Chinese Medicine, University of Macao, Macao
[h] Center for Medical Genetics, School of Life Sciences, Central South University, Changsha, Hunan, China
[i] Department of Chemistry, The Chinese University of Hong Kong, Hong Kong SAR, China

ARTICLE INFO

Keywords:
Theranostic
Alzheimer's disease
Aβ-targeting
Aβ-aggregate inhibition
3XTg-AD
5XFAD

ABSTRACT

Accumulation of amyloid-β (Aβ) oligomers and phosphorylated Tau aggregates are crucial pathological events or factors that cause progressive neuronal loss, and cognitive impairments in Alzheimer's disease (AD). Current medications for AD have failed to halt, much less reverse this neurodegenerative disorder; therefore, there is an urgent need for the development of effective and safe drugs for AD therapy. In the present study, the *in vivo* therapeutic efficacy of an Aβ-oligomer-targeted fluorescent probe, F-SLOH, was extensively investigated in 5XFAD and 3XTg-AD mouse models. We have shown that F-SLOH exhibits an efficient inhibitory activity against Aβ aggregation *in vivo*, and acts as an effective theranostic agent for the treatment of multiple neuropathological changes in AD mouse models. F-SLOH has been found to significantly reduce not only the levels of Aβ oligomers, Tau aggregates and plaques but also the levels of amyloid precursor protein (APP) and its metabolites via autophagy lysosomal degradation pathway (ALP) in the brains of 5XFAD and 3XTg-AD mice. It also reduces astrocyte activation and microgliosis ultimately alleviating neuro-inflammation. Furthermore, F-SLOH mitigates hyperphosphorylated Tau aggregates, synaptic deficits and ameliorates synaptic memory function, and cognitive impairment in AD mouse models. The mechanistic studies have shown that F-SLOH promotes the clearance of C-terminal fragment 15 (CTF15) of APP and Paired helical filaments of Tau (PHF1) in stable cell models via the activation of transcription factor EB (TFEB). Moreover, F-SLOH promotes ALP and lysosomal biogenesis for the clearance of soluble, insoluble Aβ, and phospho Tau. Our results unambiguously reveal effective etiological

Abbreviations: Alzheimer's disease, AD; amyloid-β, Aβ; amyloid precursor protein, APP; C-terminal fragment 15, CTF15; Paired helical filaments of Tau, PHF1; transcription factor EB, TFEB; autophagy lysosomal pathway, ALP; neurofibrillary tangles, NFTs; tris buffered saline, TBS; phosphate buffered saline, PBS; wild type, (WT) mice; cycloheximide, CHX; One-way analysis of variance, ANOVA; fetal bovine serum, FBS; nitrocellulose, NC; blood brain barrier, BBB; paraformaldehyde, PFA; intra-peritoneally, IP; thioflavin S, ThS; Morris water maze, MWM; contextual fear conditioning, CFC; open-field, OF; postsynaptic density protein 95, PSD-95; CsA, Cyclosporin A; TG, thapsigargin.

* Corresponding author. School of Chinese Medicine, Hong Kong Baptist University, Kowloon Tong, Hong Kong SAR, China.
** Corresponding author. Department of Chemistry, Hong Kong Baptist University, Hong Kong SAR, China.
*** Corresponding author. Department of Chemistry, The Chinese University of Hong Kong, Hong Kong SAR, China.
**** Corresponding author. School of Chinese Medicine, Hong Kong Baptist University, Hong Kong SAR, China.
E-mail addresses: ashokenviro@gmail.com (A. Iyaswamy), hungwingli@cuhk.edu.hk (H.W. Li), mswong@hkbu.edu.hk (M.S. Wong), limin@hkbu.edu.hk (M. Li).
[1] Equally contributed to this work.

https://doi.org/10.1016/j.redox.2022.102280
Received 18 January 2022; Received in revised form 27 February 2022; Accepted 5 March 2022
Available online 8 March 2022

capabilities of theranostic F-SLOH to target and intervene multiple neuropathological changes in AD mouse models. Therefore, F-SLOH demonstrates tremendous therapeutic potential for treating AD in its early stage.

1. Introduction

Alzheimer's disease (AD) is the most common form of neurodegenerative dementia. It is characterized by progressive neuronal loss and cognitive impairments including learning deficits and memory loss [1]. AD currently affects 37 million people worldwide, and the patient population is anticipated to triple by 2050, causing tremendous social and economic burdens to society [2]. Unfortunately, currently available medicines for AD provide only mild symptomatic relief; the lack of a cure is mainly due to our limited understanding of the underlying causal mechanism(s) [3]. The need for effective and safe drugs for AD is urgent [4]. The key histopathological features of AD are the accumulation of extracellular amyloid-β (Aβ) plaques and intracellular tau-associated neurofibrillary tangles (NFTs) found in the brains of AD patients [5]. Studies have shown that soluble Aβ oligomers are more toxic to neurons than plaques [6]. Aβ oligomers damage intracellular membranes leading to mitochondrial and lysosomal dysfunction, and hence resulting in oxidative stress and inefficient protein clearance by autophagy [7]. They have also been shown to be closely related to the synaptic damage that leads to the impairment in cognitive functions [6]. Studies have demonstrated that Aβ plaque formation is not correlated with disease progression; nevertheless, the level of soluble Aβ oligomers signifies that they play detrimental roles in the progression of AD [8]. Thus, reducing the level of soluble toxic Aβ oligomers and inhibiting their formation are considered to be primary promising therapeutic approaches to treating AD, particularly in the early stage [9]. Recently, an Aβ aggregate-targeting antibody, Aducanumab has raised tremendous interests in the field for reducing amyloid plaques and ameliorating cognitive decline in AD patients [10].

Meanwhile, therapeutic agents possessing a dual functionality i.e., diagnosis and treatment resulted in the emergence of theranostic probes. Theranostics is an advanced approach of developing multifunctional drugs for treating diseases including AD, as they can demonstrate enhancement of efficacy and improvement in safety of drugs [11]. Therefore, development of theranostic agents that can detect soluble Aβ oligomers and inhibit the formation of toxic Aβ oligomers would be useful for early diagnosis and treatment of AD [12]. Molecules exhibiting the dual functions of detecting and inhibiting the formation of soluble Aβ oligomers have been previously reported [13]; however, none of these molecules have shown effective *in vivo* therapeutic efficacy in alleviating Aβ pathology and improving cognitive functions in AD mouse models [14]. Since the etiology of AD is multifactorial and complex, drug candidates that can provide multiple beneficial treatment effects, such as inhibition of Aβ oligomerization and aggregation are most warranted [15]. Induction of autophagy flux to decrease Aβ oligomers and ameliorating cognitive function is another strategy to treat AD. Additionally, reduction of neuroinflammation and attenuation of synaptic deficits would be more effective and valuable strategies to treat AD, particularly in the early stage intervention [16]. However, such advanced multi-targeted drugs are currently unavailable.

Recently, we have developed a versatile theranostic agent, F-SLOH, which can selectively bind to Aβ oligomers with strong fluorescence enhancement and also easily crosses the blood-brain barrier. F-SLOH can be used for real-time visualization of Aβ in the brains of AD mice [17]. Furthermore, F-SLOH shows inhibitory effects against Aβ oligomers and aggregate formation in *in vitro* biochemical assays, and neuroprotective effects against Aβ-induced toxicity at the cellular level, suggesting it's promising potential as a therapeutic agent for AD [18,19].

The primary goal of this investigation is to demonstrate the therapeutic capabilities of F-SLOH to intervene/mitigate multiple neuropathological changes of AD in prophylactic treatment of mouse models. The effectiveness of F-SLOH to prevent and delay the AD pathology progression and treat the pathological symptoms of AD as well as its underlying mechanism are also evaluated and examined. In the present study, the multiple therapeutic beneficial aspects of F-SLOH have been experimentally demonstrated in both 5XFAD and 3XTg-AD mouse models. We have shown that the F-SLOH reduced the levels of Aβ oligomers, Aβ plaques, phosphorylated Tau aggregates, as well as APP and its metabolites in AD mouse models. F-SLOH treatment also mitigated microgliosis and reduced the reactive glial cells and astrocytes, thus alleviating neuroinflammation in 5XFAD and 3XTg-AD mice. Furthermore, F-SLOH ameliorated synaptic dysfunction and cognitive impairment in 5XFAD and 3XTg-AD mice mitigating the disease progression of AD. The significant decrease in Tau aggregates and insoluble Aβ aggregate formation after F-SLOH treatment was attributed to the promotion of autophagy and lysosomal biogenesis, involving the activation of TFEB, which resulted in mitigation of Aβ pathogenesis in both 5XFAD and 3XTg-AD mouse models. Our results unambiguously demonstrated the remarkable and multiple etiology-targeting capabilities of theranostic F-SLOH. In conclusion, F-SLOH can abrogate multiple neuropathological abnormalities in AD mouse models, and hold outstanding therapeutic potential for prophylactic and treatment applications of AD.

2. Experimental section

2.1. Antibodies and reagents

F-SLOH used in this study was synthesised as per our previous study protocol [18]. Beta Amyloid-APP (51–2700), Anti-GFAP (Z0334), β-amyloid 1–16 (803001), were purchased from Invitrogen and anti--β-Amyloid-6E10 (803003) was purchased from Biolegend. Amyloid beta-A4 (1–40) (0060-100BIOTIN/bA4(40)-5C3), Amyloid beta-A4 (1–42) (0061-100BIOTIN/bA4(42)-8G7), and Biotin-*anti*-β-Amyloid-4G8 (800706) were purchased from Nanotools. Anti-Oligomer-A11 (AHB0052), Anti-Amyloid beta Oligomer (NU1), Anti-LC3B (NB-100-2220), LAMP1(ab24170), BACE1(ab2077), p-APP (6986),TFEB (A303-673A, Bethyl), Iba1 (ab178846), p-ERK1/2 (4370P), ERK1/2 (4695P), MEK1/2 (9122S), P-p70 S6 Kinase (9205S), p70 S6 Kinase (9202S), P-4E-BP1 (2855S), 4E-BP1 (9644P), mTOR (2983S), P-mTOR (2971S), and p62 (5114S) were purchased from Novus, Abcam, Bethyl and Cell Signalling Technologies. Anti-Flag (F1804), Anti-Cathepsin D (ab75852), β-Actin (3700S), SB 216763 (1616), LY294002 (9901S), Phospho-GSK-3α/β (9331), GSK-3α/β (5676), pAKT (4060s), AKT (9272S), Histone-H3 (4499P), Anti--α-Tubulin (T8203), Alexa Fluor 488 Goat Anti-Mouse IgG (A11001), Alexa Fluor 594 Goat anti-Rabbit IgG (A11012), Alexa Fluor 488 Goat Anti-Rabbit IgG (A11008), Anti-Goat IgG HRP conjugated (HAF017), and Goat Anti-Rabbit IgG (111-035-003) were purchased from Jackson laboratories. TurboFect (R0531), Geneticin (G418-10131027), Hygromycin B (10687010), ABC Kit (PK-6100), DAB Kit (SK-4100), DEPC-Treated Water (750024), Proteinase K (3115828001), Medical X-ray film (CK04), DMEM (11965-084), PSN-Antibiotic Mixture (15640055), PVDF membrane (10600023), and Bafilomycin A1(S1413) were purchased from Thermoscientific. TRIZOL Reagent (15596018), Histobond + S slides (0810501), 10X Tris/Glycine buffer (161–0771), 10X Tris/Glycine/SDS buffer (161–0772), and Protein ladder (26616) were purchased from BioRad. Super Signal West Femto (34095), 2X laemmli sample buffer (161–0737), siRNA Human TFEB (M-009798-02-0005), and siRNA Mouse TFEB (L-050607-02-0005) were purchased from Dharmacon. TMB substrate reagent (555214),

Streptavidin/HRP (P0397), Fluorescence mounting media (S3023), Agarose (US75817), Cryomatrix (6769006), Protease inhibitor (04,693, 124 001), Phosphate buffered saline (P5368), cover glass (0107222), histo fluid mounting medium (6900002), bell-top centrifuge tubes (345829), Block ace (UK–B80), 4 x Laemmli buffer (161–0747), 2-Mercaptoethanol (M6250), and paraformaldehyde (P6148) were purchased from Sigma Aldrich. pcDNA3-HA-ERK2 WT (Plasmid # 8974) was purchased from Addgene.

2.2. Transgenic AD mice and treatment

All the animal breeding, housing and behavior experiments were performed in the laboratory animal unit of Hong Kong Baptist University. The researchers who performed all the experiments got approval from the Department of Health for performing the animal experiments in Hong Kong under the licence (20–26) in DH/HT&A/8/2/6 Pt.1. All the protocols and behavioral procedures of the study were approved by the Research Committee of Hong Kong Baptist University for the Use of Human and Animal Subjects in Research and Teaching (HASC). The 5XFAD transgenic heterozygous mice with a background of C57BL/6 were purchased from the Jackson Laboratory, USA; these mice have 3 mutations in overexpressed human APP (K670 N/M671L, I716V, V717I), and 2 mutations in human Presenilin 1 (M146L and L286V). The heterozygous 5XFAD mice were mated with wild type C57BL/6 mice, and the offspring were genotyped using tail samples to determine the positive 5XFAD mutants. The negative offspring were included in the study as the littermate wild type (WT) mice as per previous studies [20]. The 3XTg-AD mice, with a background of B6; 129, were purchased from the Jackson Laboratory, with 3 mutant protein overexpression's (K670 M/N671L, M146V, P301L). Only female 3XTg-AD mice were used for the study as per the donors' recommendations [21]. All the animal models were housed in the laboratory animal unit with controlled lighting of 12 h and with lab diet food and water for 24 h every day. Since F-SLOH showed low oral bioavailability, 5XFAD (N = 8 per group) transgenic mice were given F-SLOH (10 mg/kg or 20 mg/kg) (N = 8) intraperitoneally (IP). WT littermates were used (N = 8) ranging from 2 months of age were included in the present study. Mice were treated for 4 months. Since the 3XTg-AD mice had slow Aβ accumulation, F-SLOH was given orally with diet. The female population of 3XTg-AD transgenic mice were randomly assigned to receive either control diet (N = 8) (Lab Diet 5002) or F-SLOH (10 and 20 mg/kg) (N = 8) admixture diet from 6 to 12 months, ad libitum. Behavioral studies were performed at 6 and 12 months for 5XFAD and 3XTg-AD mice, respectively. Histopathological and biochemical analyses were conducted after sacrificing the mice.

2.3. Pharmacokinetic study

ICR Mice (30 ± 2 g) were procured and bred in the laboratory animal unit, Hong Kong Baptist University. The pharmacokinetic animal study was carried out according to the CPCSEA Guidelines. The experimental mice were fasted overnight provided with water during the experiment. A single dose of F-SLOH at dose of 20 mg/kg was IP administered to animals (n = 4 for each time point). The preparations were administered as solutions by IP at a volume of 10 mL/kg. Blood samples (500 μl) were collected from the heart of euthanized mice into heparinized centrifuge tubes at 5, 15, 30, 60,120, 240, 480, and 1440 min after drug administration. The preparation of brain samples and the plasma samples for the pharmacokinetic profiling by LC/MS is explained in detail in our previous publication [22].

2.4. Behaviour study

2.4.1. Contextual and cued fear conditioning test

The fear conditioning test was performed in both 5XFAD and 3XTg-AD mice models to check the memory function in the F-SLOH treatment group compared with Tg-Vehicle group and WT littermates. This experiment was performed using two sound-proof chambers (Ugo Basile). The experiment was performed over two days, and the memory function was evaluated by analysing the freezing time with the help of video tracking camera by ANYMAZE software. The complete experimental procedure is described in detail in our previous publication [22].

2.4.2. Open field test

The open field test is mainly used to analyse the locomotor function and degree of anxiety in the animal models during disease progression, and to assess drug efficacy in relieving these symptoms. 3XTg-AD mice were used to compare the F-SLOH treatment group with Tg-Vehicle group and WT littermates. The time spent in the margin and centre was calculated to analyse locomotor function in the specified groups. The complete experimental procedure is described in detail in our previous publication [22,23]. Behavioural data was analysed using Ethovision software version.

2.4.3. Morris water maze test

This experiment was mainly used to evaluate the learning and memory function of the experimental mice 3XTg-AD and the drug efficacy in alleviating disease pathology. At first, all experimental mice received visible platform training for four trials per day. Distance travelled or latency to climb onto the platform was measured. Then the animals were trained for 6 days in a hidden platform environment to analyse the escape latency. On the 7th day, a probe trial was performed to determine whether the mouse could remember where the platform was in the quadrant. All these experiments were recorded with an animal tracking camera, and all the behavioural data was analysed using Ethovision software. The complete experimental procedure is described in detail in our previous publication [22,23].

2.5. Dissection of AD mice brains

After the completion of memory experiments, the experimental mice were sacrificed 3 h after the last drug administration. Mice from all the groups were anaesthetized by intraperitoneal injection of 10% chloral hydrate. After perfusion, the extracted brain was dissected into two sagittal halves. One-half was immediately frozen on dry ice for quantification of Aβ by ELISA, Western analysis, whereas the other half was used for Immunohistochemistry and Golgi staining.

2.6. Determination of APP metabolites in the brain samples

An aliquot of whole brain homogenate was extracted in three different fractions namely soluble tris buffered saline (TBS) whole fraction, 1% SDS in TBS soluble fraction and insoluble formic acid fraction. These three different fractions were used for further biochemical analysis. Western blotting was used to detect soluble APP metabolites in the TBS-soluble. As for the SDS soluble fraction, ELISA was used to detect detergent soluble Aβ levels and Western blot analysis was used to detect the APP, CTF and its phosphorylated forms. Finally, formic acid insoluble fractions were analysed for insoluble $A\beta_{1\text{-}40}$ and $A\beta_{1\text{-}42}$ by ELISA. Details of the experimental procedures are described in our previous publication [22].

2.7. Determination of soluble and insoluble tau in the brain samples

An aliquot of whole brain homogenate was extracted in three different fractions namely soluble modified RIPA (S1) whole fraction, Sarkosyl soluble fraction (S2) and Sarkosyl insoluble fraction (P1). Modified RIPA (S1) whole fraction with protease inhibitors and phosphate inhibitor cocktail tablets were used for further phospho Tau extraction. The brain homogenate was centrifuged at 110,000 for 30 min to separate soluble (S2 fraction, non-pathogenic Tau) and insoluble pellets. The homogenate was incubated with 1% sarkosyl at 37 °C for 2 h

at room temperature. Next, the samples were centrifuged at 110,000 for 30 min to separate sarkosyl-insoluble Tau in the pellet (P1 fraction). The pellet (P1) was resuspended in Tris-EDTA buffer (20 μl). S2 and P1 fractions were used for the detection of HT7, CP13, AT8, PHF-1 and MC-1.

2.8. Western blot analysis (WB)

Immunoblot was used to determine protein levels in the soluble and insoluble fractions of the whole brain homogenate. The cell and animal brain homogenates were equalised by protein estimation and run in the respective percentage of gel as per the required target protein. Then the target protein was transferred to the PVDF membrane in a BIORAD transfer apparatus. The membrane was blocked in 5% milk for 1 h and washed twice with TBST. Then the membrane was incubated with target primary antibody overnight in a cold room at 4 °C with constant shaking. Next day the primary antibody was collected. The membrane was washed with TBST and incubated with target secondary antibody for 1 h. The membrane was washed in TBST twice for 10 min each and developed with Super Signal West Pico or Femto kit. The chemiluminescent signals in the membrane were developed with the medical film in a dark room. The signals were confirmed by band intensity analysis using Image J software. The complete experimental procedure is described in our previous publication [22].

2.9. Immunohistochemistry (IHC)

Experimental animals were perfused with phosphate buffered saline (PBS). The brains were extracted and cut into two halves sagittally. One of the halves was fixed in 4% paraformaldehyde (PFA) and stored at 4 °C for 24 h. Next day the PFA was removed, and the tissue was washed with PBS twice and incubated in 30% sucrose for 2–3 days until the tissues sank completely. Brain tissue was sectioned with a cryotome into 30-μm slices. All the brain slices were soaked in PBS with 0.4% Triton X100 and incubated for 2 h for free-floating staining. Selected regions of hippocampus brain slices were washed in PBS, and the free-floating sections were incubated in 3% H2O2 for 10 min to quench the endogenous peroxidase activity. Then the brain slices were washed twice in PBS and blocked in 2.5% bovine serum albumin (BSA) for 2 h. Then the BSA was removed and the target primary antibody biotinylated 4G8 was added and incubated overnight at 4 °C in a cold room. Next day the primary antibody was collected, and brain slices were washed twice in PBS and incubated with ABC reagent for 2 h. Then the brain slices were washed twice with PBS and incubated in DAB reagent for 10 min until they turned light brown. The reaction was stopped by diluting the DAB reagent with water. Then the free-floating brain slices were gently removed with a paint brush and placed in water on coated slides. The water on the slides was removed leaving the brain slices fixed on the slides. The slides were dried in an oven at 55 °C for 20 min. The slides were processed in an alcohol series to remove water, cleared by xylene and mounted with mounting medium under a coverslip. Different regions of brain slice were photographed under the microscope, and images were analysed using Image J software. The complete experimental procedure is described in our previous publication [22,24].

2.10. ELISA

The SDS fraction of the brain homogenate was used as the soluble fraction, and the formic acid fraction was used as the insoluble fraction for the Aβ analysis [25]. All these fractions were subject to protein estimation and equalised with the extraction buffer, and then used for ELISA experiments to determine the $A\beta_{1\text{-}40}$ and $A\beta_{1\text{-}42}$ content. A 96-well plate was incubated with 6E10 primary antibody in phosphate buffer at 4 °C overnight in a cold room. Next day the primary antibody was collected; the plate was washed with PBST twice and gently tapped to remove excess solution. Then the plate was incubated with block ACE for 1 or 2 h, washed twice with PBST and gently tapped to remove excess liquid in the wells. Soluble and insoluble fractions of the brain homogenate were added to the marked wells with standard peptides of Aβ and incubated for 2 h with mild shaking. Then the samples were removed and washed twice with PBST and incubated with secondary antibody for 1 h with shaking. Plates were washed with PBST twice and gently tapped, and the wells were incubated with Streptavidin HRP for 30 min. Then the plates were washed thrice with PBST and gently tapped on tissue paper to remove excess liquid in the wells. The wells were filled with TMB substrate and placed in the dark until blue colour appeared. Wells in the plates were filled with 2 M H_2SO_4, changing the colour from blue to yellow, and the absorbance was read in the 96-well plate reader at 450 nm. The samples were assessed by comparing results with the Aβ peptide standard curve. The complete experimental procedure is described in our previous publication [22].

2.11. Golgi staining and morphological analysis of dendritic spines

After the animals had been perfused with phosphate buffered saline (PBS), the brains were extracted and cut into two halves sagittally [26]. One of the halves was fixed in the Solution AB (mercuric chloride, potassium dichromate, and potassium chromate) provided in the FD Rapid Golgi Stain Kit for two weeks at room temperature. The Solution AB was changed two times. The Solution AB was replaced by Solution C (Potassium Chromate) for 3 days. Tissue was washed twice with distilled water and sectioned in cryotome. Brain slices were placed on the coated slides to remove Solution C and dried at room temperature for two days. The slides were washed with water twice and then incubated in Solution DE for 10 min. Slides were washed twice in water and incubated in different concentrations of alcohol to remove the water in tissue. Finally, the brain slices on the slides were cleared with xylene and mounted with coverslip using mounting media. The spines and dendrites were photographed under a microscope and analysed for spine density and spine morphology using NIH Image J Sholl software.

2.12. In vitro studies

HeLa cells, CHO 7PA2 cells, HT-22 cells and N2a cells were cultured in DMEM media supplemented with 10% fetal bovine serum (FBS) and 50 units of PSN mixture. All the cells were cultured in the above specified media at 37 °C in a CO_2 Incubator and used for different experiments. N2a cells were transiently transfected with human APP Swe/Ind (APP 695 Swedish/Indiana mutation) (30145, Addgene) with transfection reagent, Turbofect to obtain a 70–80% transfection efficiency. The same steps were repeated for transfecting P301L-Tau (46908, Addgene) plasmids. Then the transfected cells were treated with F-SLOH (6.25, 12.5 and 25 μm) for 24 h. Cell lysates were collected for protein analysis. HeLa cells stably expressing 3XFlag TFEB to be used for immunocytochemistry were maintained in DMEM with 10% FBS and 50 U PSN, along with 100 μg/ml Geneticin (G418).

2.13. Transfection experiments

For both knock down and overexpression experiments HeLa, HT-22 and N2a cells were transfected with human or mouse target siRNA by using RNAiMAX (13778030) purchased from Invitrogen. Cells were incubated for at least 48 h for better transfection efficiency. For overexpression experiment the target plasmids were transfected with TurboFect (R0531). Cells were incubated for at least 48 h for better transfection efficiency. Transfected cells were treated with F-SLOH at indicated concentrations.

2.14. Immunocytochemistry

For the cell staining experiments HT-22 or HeLa cells were seeded on round coverslips placed in a 24-well plate for 24 h. After the cells had

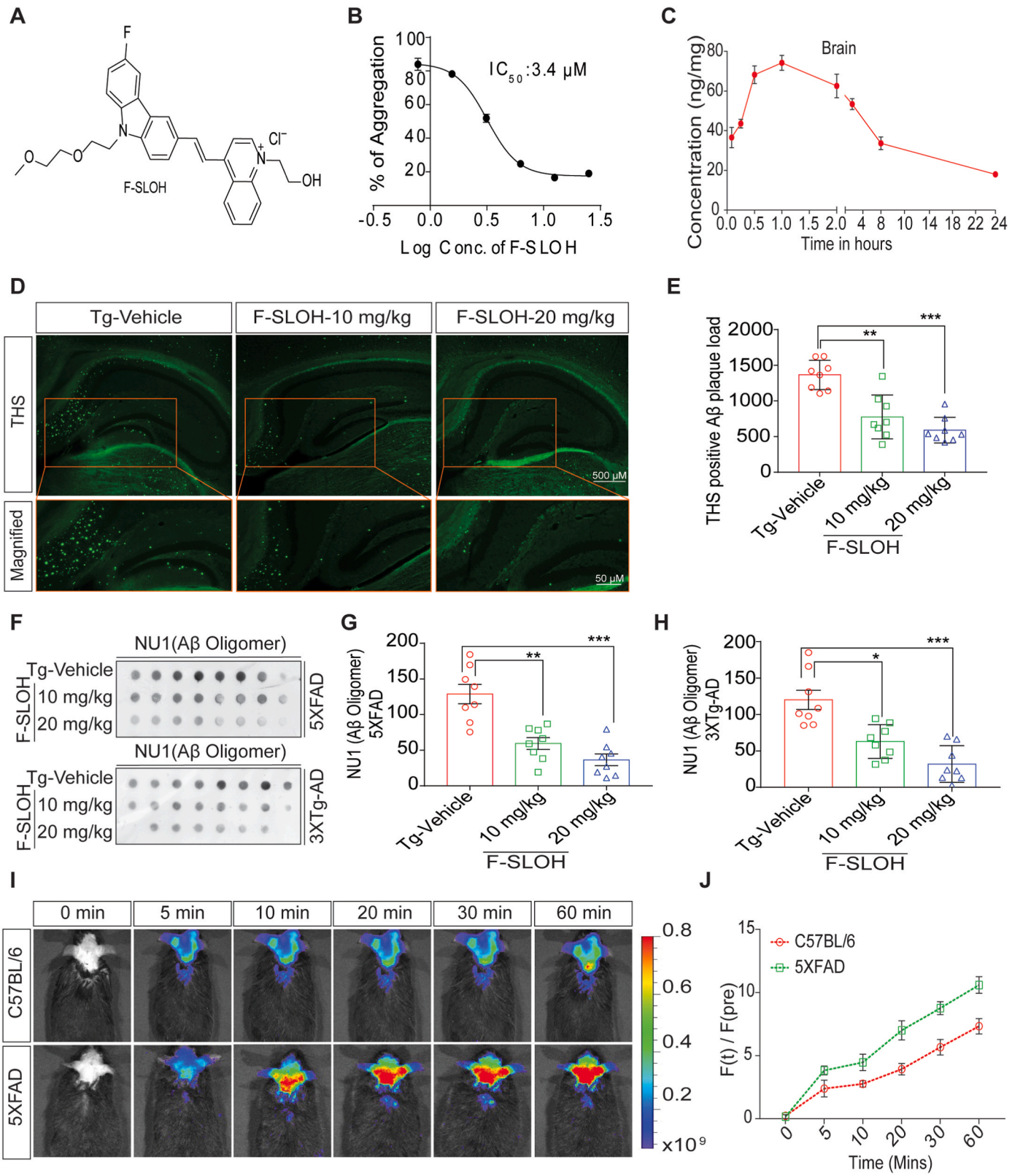

Fig. 1. F-SLOH binds to Aβ species, inhibits Aβ fibrillation *in vitro* and reduces Aβ monomers, oligomers and plaques in preclinical AD animal models. (A) Chemical structure of F-SLOH. (B) F-SLOH dose-dependently inhibited the fibril formation of Aβ in the ThT anti-Aβ fibrillation fluorescence assay. The IC_{50} value of anti-fibrillation activity of F-SLOH is 3.4 μm. (C) Pharmacokinetic properties of F-SLOH. Concentration vs time after intraperitoneal administration at a dose of 20 mg/kg/d in brain tissue of ICR mice (N = 4). (D) F-SLOH treatment mitigates ThS-positive Aβ plaques in 5XFAD brain slice. F-SLOH (10 and 20 mg/kg) treatment reduces the ThS-positive plaques in 5XFAD mice when compared to Tg-vehicle and (E) its corresponding quantification. (F) Levels of NU1 (Aβ oligomer) presented in the dot blot representing treatment effects of F-SLOH (10 and 20 mg/kg) and its corresponding quantification of Aβ oligomers found in the brain lysates of (G) 5XFAD and (H) 3XTg-AD mice. Quantified data presented as mean ± SEM. N = 8. (I) Intra-peritoneal (IP) injection of F-SLOH (20 mg/kg) in 5XFAD mice and WT mice were observed using *in vivo* imaging in small animal imaging system (J) and its corresponding quantification.

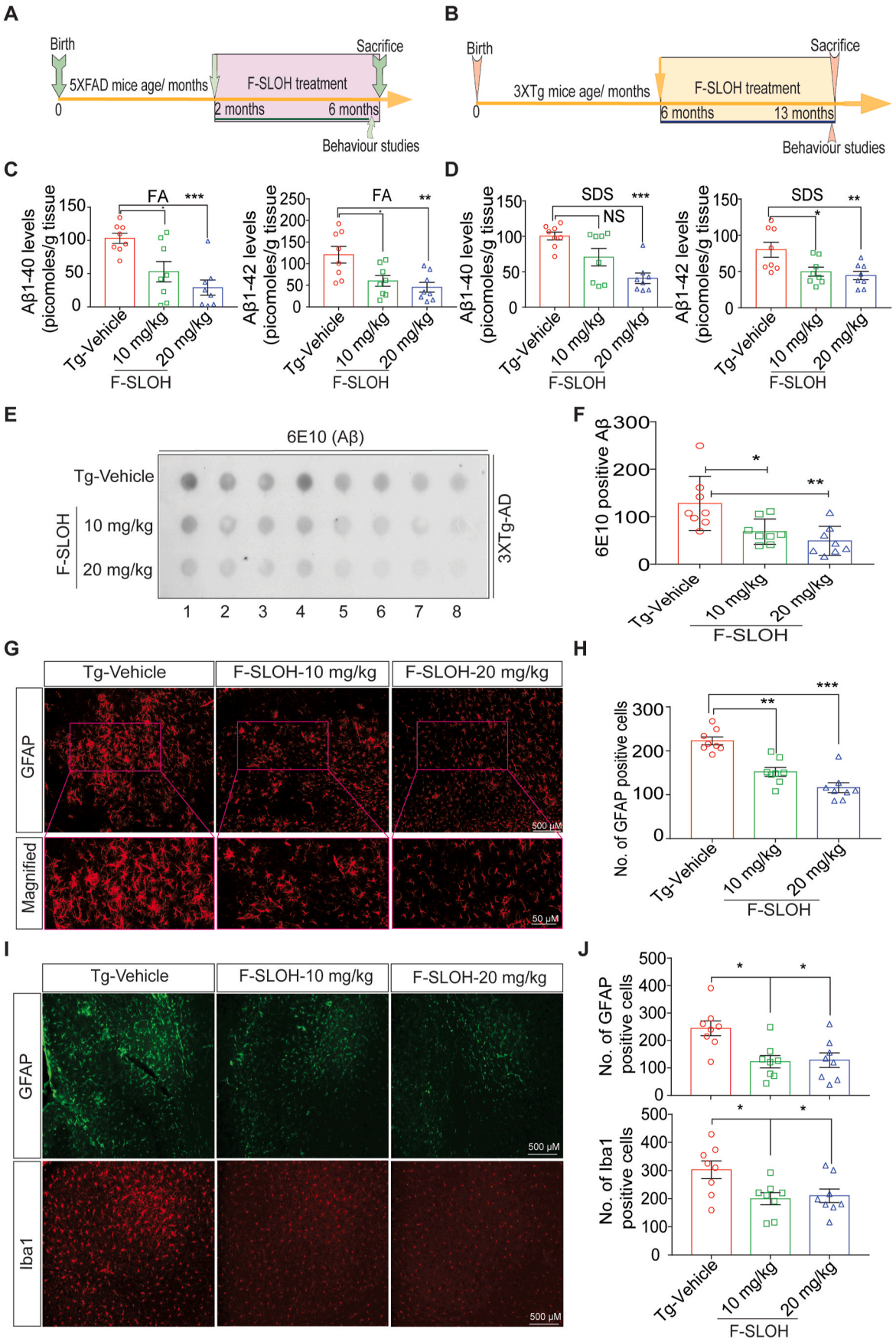

(caption on next page)

Fig. 2. F-SLOH reduces astrocytic activation and microgliosis and ameliorates neuroinflammation in the brains of AD model mice. Timeline of F-SLOH treatment and behaviour experiment schedule for (A) 5XFAD and (B) 3XTg-AD transgenic mice. (C) F-SLOH treatment reduced $A\beta_{1\text{-}40}$ and $A\beta_{1\text{-}42}$ levels in the formic acid soluble brain lysates and its corresponding quantification in 5XFAD mice. (D) F-SLOH treatment reduced $A\beta_{1\text{-}40}$ and $A\beta_{1\text{-}42}$ levels in the SDS soluble brain lysates and its corresponding quantification in 5XFAD mice. (E) The protein levels of 6E10 (Aβ) presented in the dot blot representing treatment effects of F-SLOH (10 and 20 mg/kg) (F) and its corresponding quantification in 3XTg-AD mice brain lysates. (G) F-SLOH treatment (10 and 20 mg/kg) reduced the GFAP positive reactive astrocytes in the brain slice of 5XFAD transgenic mice and (H) its corresponding quantification (I) Chronic treatment of F-SLOH (10 and 20 mg/kg) reduced the levels GFAP and Iba1 positive reactive glial cells and reactive astrocytes in the brain slices and (J) its corresponding quantification of 3XTg-AD mice. Quantified data presented as mean ± SEM. N = 8.

attached, indicated drugs were added and incubated for 24 h. Then the plates were placed in ice, the media was removed from the wells, cells were washed with PBS, and fixed with 4% PFA for 15 min. Cells were washed with PBS twice and incubated with 0.4% TritonX100 in PBS for 10 min. Further, cells were blocked with 5% BSA for 30 min. Next the BSA was removed, and the target primary antibody was added, and cells were incubated overnight at 4 °C in a cold room. Next day the primary antibody was collected and the cells were washed with PBS. The fluorescent secondary (488 or 594) antibody was added for 2 h. Finally, the coverslips were washed in PBS twice, mounted on the slides, and photographed using a confocal microscope for further analysis.

2.15. Lysotracker experiment

For the lysotracker experiments, drug-treated cells were incubated with 50 nM of LysoTracker Green DND99 (Thermo Scientific) for 1 h. Cells were washed with PBS, treated with trypsin and then collected. The cells were collected in centrifuge tubes with 100 μl PBS and analysed using a flow cytometer. The data was analysed by the Flow Jo software.

2.16. Quantitative real time PCR

The treated cells were washed with PBS and treated with trypsin to collect the cells in the tube containing 100 μl of TRIZOL reagent. The total RNA was extracted using the protocol mentioned in the kit and quantified using Nanodrop (Thermo Scientific). The RNA was converted to cDNA using the cDNA conversion kit (Invitrogen). cDNA, the target primer for autophagy and TFEB target genes were processed with master mix (SYBR Green master mix, Life Technologies, 4385612) using a PCR system. Results were analysed as per instruction for the CT method, considering the internal control GAPDH, and normalized.

2.17. Dot blot assay

The SDS fraction of the brain homogenate was used as the soluble fraction, and formic acid fraction was used as the insoluble fraction for Aβ analysis. Both fractions were subject to protein estimation and equalised with the extraction buffer. The dot blot apparatus (BioRad) was rinsed in MilliQ water twice and arranged as per the protocol. The nitrocellulose (NC) membrane was cut as per the size of the 96 wells and rinsed in PBS. Then the NC membrane was placed above the rubber sheet of the apparatus, sandwiched with the 96-well cover plate, and attached by suction with a vacuum pump. The membrane suction efficiency was checked twice. When vacuum was achieved, all 96 wells were loaded with samples and left for 10 min to ensure that protein was transferred to the NC membrane. The NC membrane was removed from the apparatus and blocked in 5% milk for 1 h. Then the milk was removed followed by two washes in TBST, and the target primary antibody 6E10 or NU1 was incubated at 4 °C overnight in a cold room. Next day the primary antibody was collected followed by two washes with TBST, and the target secondary antibody was incubated for 1 h. Finally, the NC membrane was developed with a chemiluminescent kit and the dot intensity was analysed using Image J software.

2.18. Statistical analysis

All data in the bar diagram are represented as mean ± SEM calculated using GraphPad Prism software. The comparison of groups and the significance between the groups was illustrated using One-way analysis of variance (ANOVA) following Dunnett's multiple comparison between groups. Further analysis of differences between the animals and between the groups were done with two-way ANOVA with multiple comparison. A probability value of $P < 0.05$ was statistically significant when comparing groups and animal samples.

3. Results

3.1. F-SLOH binds to Aβ species, inhibits Aβ fibrillation in vitro and reduces Aβ monomers, oligomers and plaques in preclinical AD animal models

We have previously shown that F-SLOH (Fig. 1A) is an effective and sensitive diagnostic probe for *in vivo* imaging of Aβ aggregates and plaques in AD mouse models in the early stage. To further confirm the binding capability of F-SLOH toward Aβ species in the brains of 5XFAD mice, F-SLOH was IP injected and detected at different time points and compared with the WT littermates. *Ex vivo* colocalization studies of F-SLOH using Aβ plaque-specific thioflavin S (ThS) dye, oligomer-specific A11, Aβ-specific 6E10 and 4G8 antibodies were performed. Both *in vivo* (Fig. 1I and J) and ex vivo (Supplementary Fig. S1D, S1E and S1F) images show the excellent targetability of F-SLOH toward Aβ oligomers and plaques. Furthermore, the inhibitory efficiency of F-SLOH against Aβ aggregation was determined by the Thioflavin T (ThT) anti-Aβ fibrillation fluorescence assay. The results indicate that F-SLOH dose-dependently inhibited Aβ fibril formation with the IC_{50} value of 3.4 μm (Fig. 1B), suggesting its therapeutic potential. The blood-brain barrier (BBB) permeability and bioavailability of F-SLOH in the brain are also crucial for successful treatment. The results of pharmacokinetic studies clearly demonstrated that F-SLOH was BBB permeable (Fig. 1C) and bioavailable in brain and plasma (Supplementary Fig. S1A) with a C_{max} 81.134 ng/g and T_{max} of 1 h (Supplementary Fig. S1B). All these desirable properties facilitate F-SLOH for further investigation of *in vivo* therapeutic studies.

Accumulation of Aβ oligomers and aggregates is a crucial pathological event or factor in the progression of AD. To determine whether F-SLOH could therapeutically reduce Aβ oligomers and Aβ plaques in preclinical AD mouse models including 5XFAD and 3XTg-AD mice, F-SLOH was intraperitoneally or orally administrated on alternate days for 4 and 7 months, respectively. The whole therapeutic study is illustrated in a timeline graph presented in Fig. 2A and B for 5XFAD and 3XTg-AD mouse models, respectively. During the treatment, F-SLOH did not cause any abnormal changes in animal body weight or behaviour (Supplementary Figs. S2A and S2B). After behavioural experiments, the F-SLOH-treated mice were sacrificed, and their brains were extracted for histopathology and biochemical analyses. ThS staining was used to label the extracellular Aβ plaque load in brain slices. As shown in Fig. 1D and E, the Aβ plaque deposits were dramatically reduced in the hippocampus and whole brain of the F-SLOH-treated AD model mice as compared to those of the Tg-Vehicle-treated mice. Notably, the reduction of Aβ plaques was consistent in both 5XFAD and 3XTg-AD mouse models (Supplementary Fig. S1C). To evaluate Aβ content in brain slice and brain SDS lysate fractions of the tested mice, immunohistochemistry and dot blot assays were performed using 4G8 and 6E10 antibodies, which identify all Aβ species and recognizes APP in the cellular content.

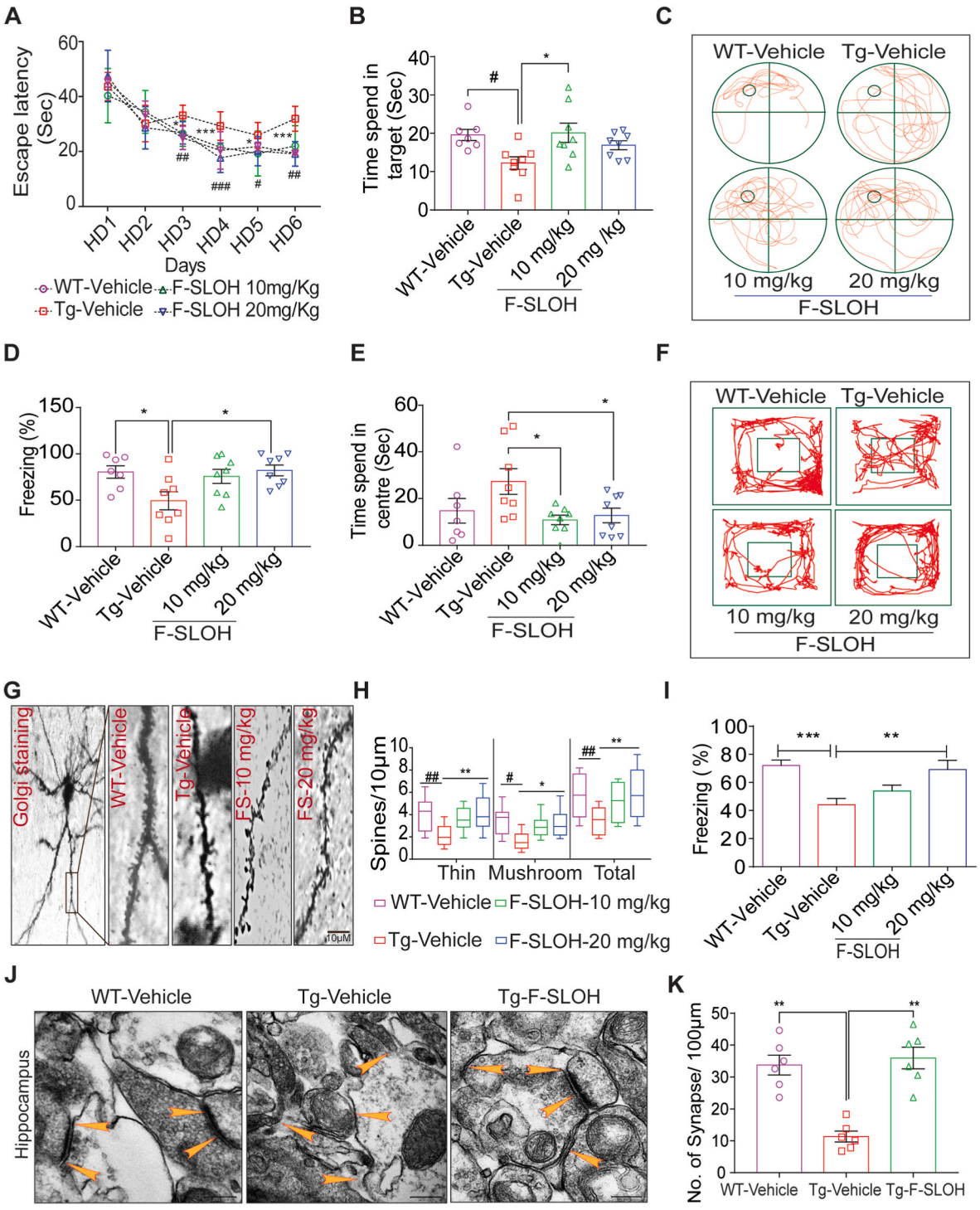

Fig. 3. F-SLOH treatment improves spatial learning, memory function and augments synapse formation in AD mouse models. (A) F-SLOH-treated 3XTg-AD mice improved the spatial escape rate and decreased the escape latency during the learning period of six days in Morris water maze test when compared to the Tg-Vehicle group (N = 8). (B) F-SLOH-treated mice probed the platform placed quadrant for longer time when compared to the vehicle-treated Tg mice in the probe trial. (C) The images illustrate the animal's behaviour on the probe trial using video tracking software. (D) F-SLOH improves hippocampal-dependent memory and memory in F-SLOH-treated 3XTg-AD mice in comparison to the vehicle-treated Tg mice using contextual fear conditioning. (E) F-SLOH treatment improved exploratory behaviour and locomotor activity in open field experiment when compared to the Tg-Vehicle and its corresponding quantification. (F) Images illustrating the animal's locomotor behaviour in open field experiment using video tracking software. (G) Golgi staining of brain hippocampal slice from the F-SLOH-treated 3XTg-AD mice and Tg vehicle. (H) Data show an increase in thin and mushroom structures of spines along with total length of the spines when compared between the Tg-vehicle group and F-SLOH treatment (10 and 20 mg/kg) groups in a dose-dependent manner, indicating improved spinogenesis. (I) F-SLOH improved hippocampal-dependent memory in F-SLOH-treated 5XFAD mice when compared to the vehicle-treated Tg mice using contextual fear conditioning. (J) F-SLOH treatment ameliorates hippocampal-dependent synapse formation in the brain slices of 5XFAD mice. The ultrastructure of the synapse displayed in electron micrograph indicates that F-SLOH treatment improved the synapse formation in comparison to the vehicle-treated Tg group. (K) Quantification of number of synapses in the brain slice of 5XFAD mice. Quantified data presented as mean ± SEM. N = 8.

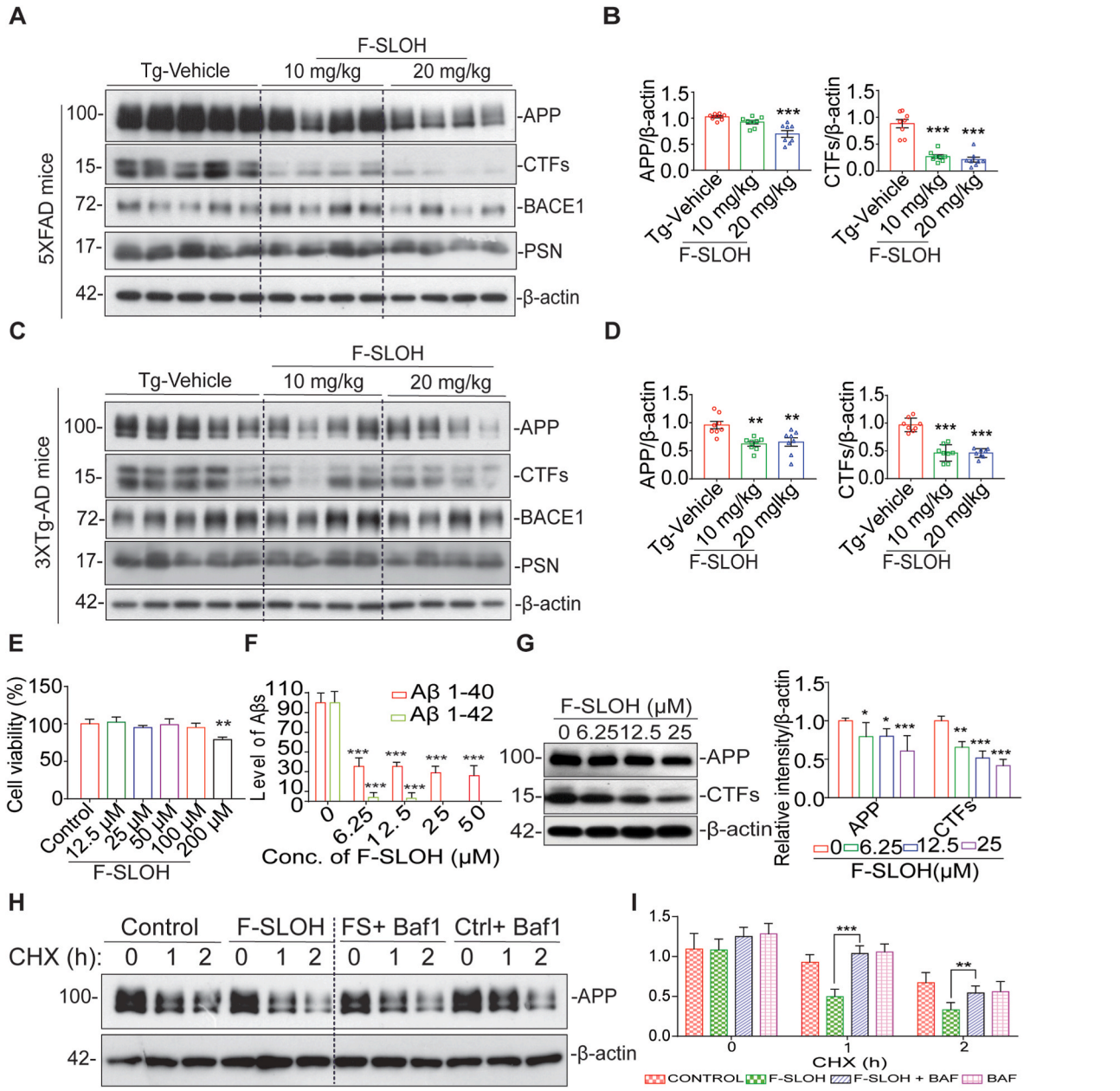

Fig. 4. F-SLOH alleviates APP processing in AD mouse models. (A) F-SLOH treatment (10 and 20 mg/kg) reduces the protein expression levels of FL-APP and CTFs in the brain lysates of 5XFAD mice shown in immunoblot (B) and its corresponding quantification. (C) Chronic F-SLOH treatment reduced the protein expression levels of FL-APP and CTFs in the brain lysates of 3XTg-AD mice independent of BACE1, presenilin inhibition are shown in immunoblot and (D) its corresponding quantification. Quantified data presented as mean ± SEM. N = 8. (E) The cell viability test of F-SLOH on N2a cells overexpressing APP695 (N2a-APP) was determined using the MTT and its corresponding quantification. (F) F-SLOH treatment (6.25, 12.5, 25 and 50 μM) reduced the $A\beta_{1-40}$ and $A\beta_{1-42}$ protein expression levels in the cell media and its corresponding quantification. Each data represents the average of three replicates. (G) F-SLOH treatment (6.25, 12.5 and 25 μM) in N2a-APP cells significantly reduced the protein expression levels of FL-APP and CTFs and its representative blots are shown with its corresponding quantification. (H) F-SLOH mediated reduction of full-length APP were significantly blocked after BafA1 treatment at the indicated timepoint of CHX treatment in N2a-APP cells and its representative blots are shown with its (I) corresponding quantification. Each data represents the average of three replicates and data represented as mean ± SEM.

Consistently, the Aβ level was dramatically reduced in the hippocampus and whole brain slices of the F-SLOH-treated group in a dose-dependent manner when compared to those of the Tg-Vehicle-treated group (Supplementary Figs. S2C and S2D) of 5XFAD mice. Such reduction was also found in 3XTg-AD mouse models (Supplementary Figs. S2E and S2F). Dot blot analysis with 6E10 antibody showed that F-SLOH significantly decreased the levels of Aβ species in the 3XTg-AD mouse model (Fig. 2E and F). Studies have shown that Aβ oligomers play a major role in inducing the neuronal and synaptic loss during AD disease progression because of their higher toxicity [27,28]. The dot blot assays were also performed with Aβ oligomer-specific NU1 antibody to evaluate the capability of F-SLOH to reduce Aβ oligomers in mouse models. Indeed, F-SLOH significantly decreased the levels of oligomeric Aβ species in the insoluble homogenate brain fraction in both 5XFAD and 3XTg-AD mice (Fig. 1F, G and1H). Meanwhile, the level of $A\beta_{1-40}$ and $A\beta_{1-42}$ in the SDS (soluble) and formic acid (insoluble) fractions of brain lysates was determined using ELISA. F-SLOH treatment significantly decreased the $A\beta_{1-40}$ and $A\beta_{1-42}$ levels in the soluble and insoluble brain fractions of 5XFAD mice when compared with the Tg-Vehicle group. This clearly demonstrated that F-SLOH could also reduce the monomeric Aβ species

(Fig. 2C and D). In short, F-SLOH can not only target Aβ species but also effectively reduce Aβ monomers, oligomers as well as Aβ accumulation and deposition in AD mouse models.

3.2. F-SLOH reduces astrocytic activation and microgliosis, ameliorating neuroinflammation in brains of AD model animals

Studies have reported that chronic neuroinflammation has been found in the brains of AD patients implying that Aβ plaques can activate the astrocytes and microglia causing inflammation [29]. To examine whether the reduction of Aβ by F-SLOH treatment can ameliorate neuroinflammation in 5XFAD and 3XTg-AD mice, their brain slices were stained with GFAP and Iba1 antibodies which detect astrocytes activation and microgliosis, respectively. As expected, F-SLOH treatment markedly reduced astrocytic activation and microgliosis in 5XFAD (Fig. 2G and H) and 3XTg-AD mice as compared to the Tg-Vehicle-treated mice (Fig. 2I and J). In summary, our results unambiguously showed that treatment with F-SLOH reduced intracellular levels of Aβ species including oligomers, reduced extracellular Aβ accumulation, and markedly suppressed neuroinflammation in the brains of 5XFAD and 3XTg-AD model mice in a dose-dependent manner.

3.3. F-SLOH treatment improves spatial learning, memory function and augments synapse formation in AD mouse models

It is widely believed that aggregation of Aβ is an important pathological event and is closely related to the synaptic dysfunction and memory decline leading to loss in neuronal plasticity and neurodegeneration in AD [30]. To investigate whether F-SLOH treatment could improve the learning and memory function of 5XFAD and 3XTg-AD mouse models, several behavioural tests including Morris water maze (MWM), contextual fear conditioning (CFC), and open-field (OF) tests were performed. Golgi staining was adopted for dendritic spine density and synaptic structure investigations. All the experimental mice used in the study were subject to MWM visual training for one day to assess their swimming efficiency and vision capacity. Next, for 6 days, the hidden platform was used to train all the experimental mice. During the learning sessions, the WT mice learned faster and showed a short escape latency as compared to the Tg-Vehicle-treated mice (Supplementary Fig. S3A) clearly illustrating that the Tg-Vehicle group had learning deficits. F-SLOH treatment rescued the learning impairment in 3XTg-AD mice which showed a shorter latency to escape when compared to the Tg-Vehicle mice (Fig. 3A). After the hidden platform test, all the mice were subject to the memory recovery test in probe trial. The F-SLOH-treated group spent more time in probing the platform in the target quadrant when compared to the Tg-Vehicle group (Fig. 3B and C). The results of MWM clearly demonstrated that F-SLOH rescued learning and memory impairment in 3XTg-AD mice. In addition, the CFC test was used to evaluate the effect of F-SLOH on hippocampal memory in 3XTg-AD and 5XFAD mice. The 2-day training with pre-shock, 24-h context and 24-h cue-tone assessments were performed. Results clearly demonstrated that F-SLOH treatment groups exhibited a prolonged freezing time with improved memory function in the hippocampus when compared with the Tg-Vehicle group of 3XTg-AD and 5XFAD mice (Fig. 3D and I). The open field experiment was also conducted to assess locomotor function and anxiety of the 3XTg-AD mice. During the 5-min assessment, the F-SLOH-treated mice were very active in the novel environment and showed more interest in exploring when compared to the Tg-Vehicle counterparts (Supplementary Fig. S3B). The Tg-Vehicle mice were frightened of the novel environment and spent more time (inactive) in the centre (Fig. 3E and F). These results clearly demonstrated F-SLOH improved the exploratory and locomotor function in 3XTg-AD mice. The memory deficits in AD can be traced back to the presence of Aβ oligomers. The oligomers impair synaptic plasticity and cause neuronal degeneration; this leads to abnormal neuronal circuit activity, which in turn disturbs homeostatic firing in the hippocampus [31]. To assess the effect of F-SLOH on dendritic spine density and synaptic structures, the Golgi staining of brain slices of 3XTg-AD mice using an FD Golgi staining kit was performed. The images of dendritic spines of the F-SLOH-treated group revealed (Fig. 3G and H) increases in the formation of mushroom spines with developed synaptic connections and in spine density when compared with the Tg-Vehicle group. The protein expression levels of postsynaptic density protein 95 (PSD-95) and synaptophysin were also investigated. F-SLOH-treated 3XTg-AD (Supplementary Figs. S3C) and 5XFAD (Supplementary Fig. S3D) mice showed higher expression levels of PSD-95 and synaptophysin as compared to the untreated Tg-Vehicle group. F-SLOH treatment also ameliorated hippocampal-dependent synapse formation in the brains of 5XFAD mice as shown in Fig. 3J and K. The ultrastructure of the synapse as shown in electron micrographs indicated that F-SLOH treatment increased synapse formation as compared to the Tg-vehicle group. These collective findings consistently demonstrate that F-SLOH restores dendritic spine density and increased the formation of synaptic plasticity between neurons in hippocampus rescuing the learning and memory impairment in mice of both 3XTg-AD and 5XFAD models.

3.4. F-SLOH alleviates APP processing in AD mouse models

Proteolytic APP processing generates Aβ, which is deposited in AD brains. The toxic Aβ deposition causes mutations, which in turn trigger even greater production of Aβ [32]. The above findings demonstrate that F-SLOH can reduce Aβ content and deposition in 3XTg-AD and 5XFAD mouse models. We further investigated APP processing and its metabolites in the brain homogenates of 3XTg-AD and 5XFAD mice using immunoblotting. The half hemisphere of the brain was differentially extracted into three fractions, namely TBS-soluble, SDS-soluble and formic acid-soluble. The SDS-soluble fraction was used to detect APP metabolite proteins in order to assess the level of proteolytic APP processing in the tested mice. As shown in Fig. 4A, B, 4C and 4D, the F-SLOH-treated group showed significant reduction in the full-length APP and its metabolite CTFs in the SDS-soluble brain fractions of 3XTg-AD and 5XFAD mice independent of BACE1 when compared with Tg-Vehicle. The exacerbated APP induces the accumulation of immature APP and it causes defects in the degradative pathways, such as autophagy, leading to cellular damage [33]. F-SLOH treatment significantly reduced APP and CTFs, clearly demonstrating that it had reduced accumulation of immature APP in the cells by inducing the degradation of the APP metabolites. Furthermore, we evaluated the APP metabolites in AD cell models, F-SLOH was non-toxic even at high concentration in the N2a-APP cells (Fig. 4E). F-SLOH (6.25, 12.5 and 25 μM) significantly reduced protein levels of full-length APP, metabolite CTF, and $A\beta_{1-42}$ in the treated N2a-APP cells (Fig. 4F and G), 7PA2 cells (Supplementary Figs. S4A and S4B) in a dose-dependent manner consistently demonstrating its *in vitro* efficacy in clearing APP metabolites. Proteolytic APP processing is dependent on BACE1 and Presenilin in AD pathogenesis. So, we verified whether F-SLOH mediated reduction of full-length APP and CTFs is due to the proteolytic mechanism of APP. Unfortunately, F-SLOH mediated reduction of full-length APP is not dependent on BACE1 (Fig. 4A and C) and presenilin induced proteolytic APP processing. Next to understand the mechanism of F-SLOH-mediated reduction of full-length APP, we investigated the mRNA levels of APP by qPCR analysis. Intriguingly, there was no change in the mRNA levels of APP after the F-SLOH treatment (data not shown). From the above mRNA analysis, it is confirmed that F-SLOH treatment only reduced the full-length APP protein without affecting the mRNA levels in AD cell and animal models. The exacerbated APP induces the accumulation of immature APP and causes defects in the degradative pathways leading to cellular damage [31]. So, we verified whether F-SLOH mediated reduction of full-length APP is dependent on lysosomal degradation of APP. We employed cycloheximide (CHX) to inhibit protein synthesis and co-treated with bafilomycin A1 (BafA1) to prevent lysosomal acidification. It was interesting to find that F-SLOH-mediated reduction of

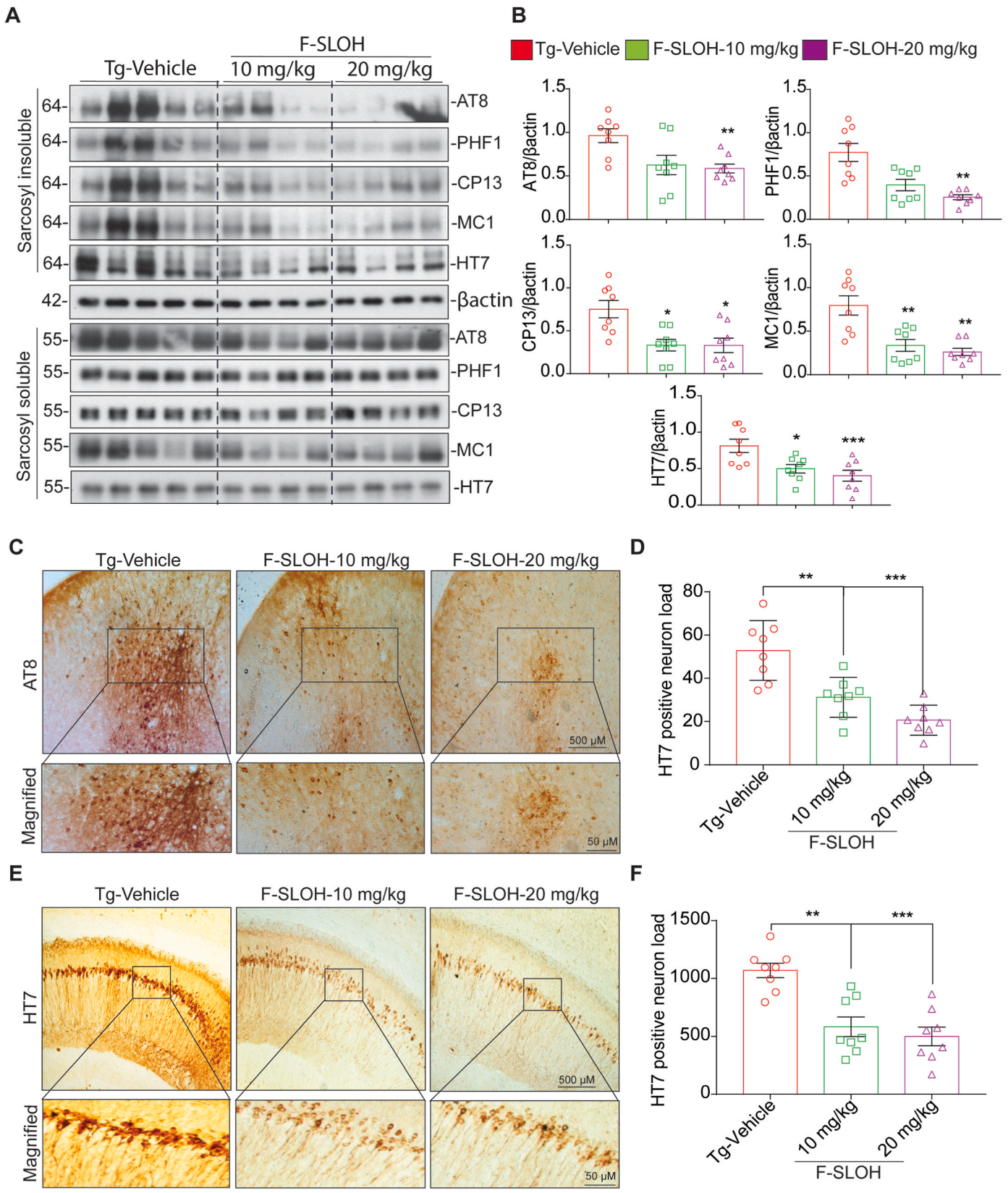

Fig. 5. F-SLOH mitigates tau pathology in 3XTg-AD mouse model. (A) Chronic F-SLOH treatment reduced the insoluble phospho Tau protein expression levels of PHF1, CP13, MC1, AT8, and HT7 in the brain lysates of 3XTg-AD mice but not the soluble phospho Tau are shown in immunoblot and (B) its corresponding quantification. (C&E) F-SLOH treatment mitigates AT8 and HT7 positive neuronal load in 3XTg-AD mice brain slice. F-SLOH (10 and 20 mg/kg) treatment reduces the AT8 and HT7 positive neuronal load in 3XTg-AD mice when compared to Tg-vehicle and (D&F) its corresponding quantification. Quantified data presented as mean ± SEM. N = 8.

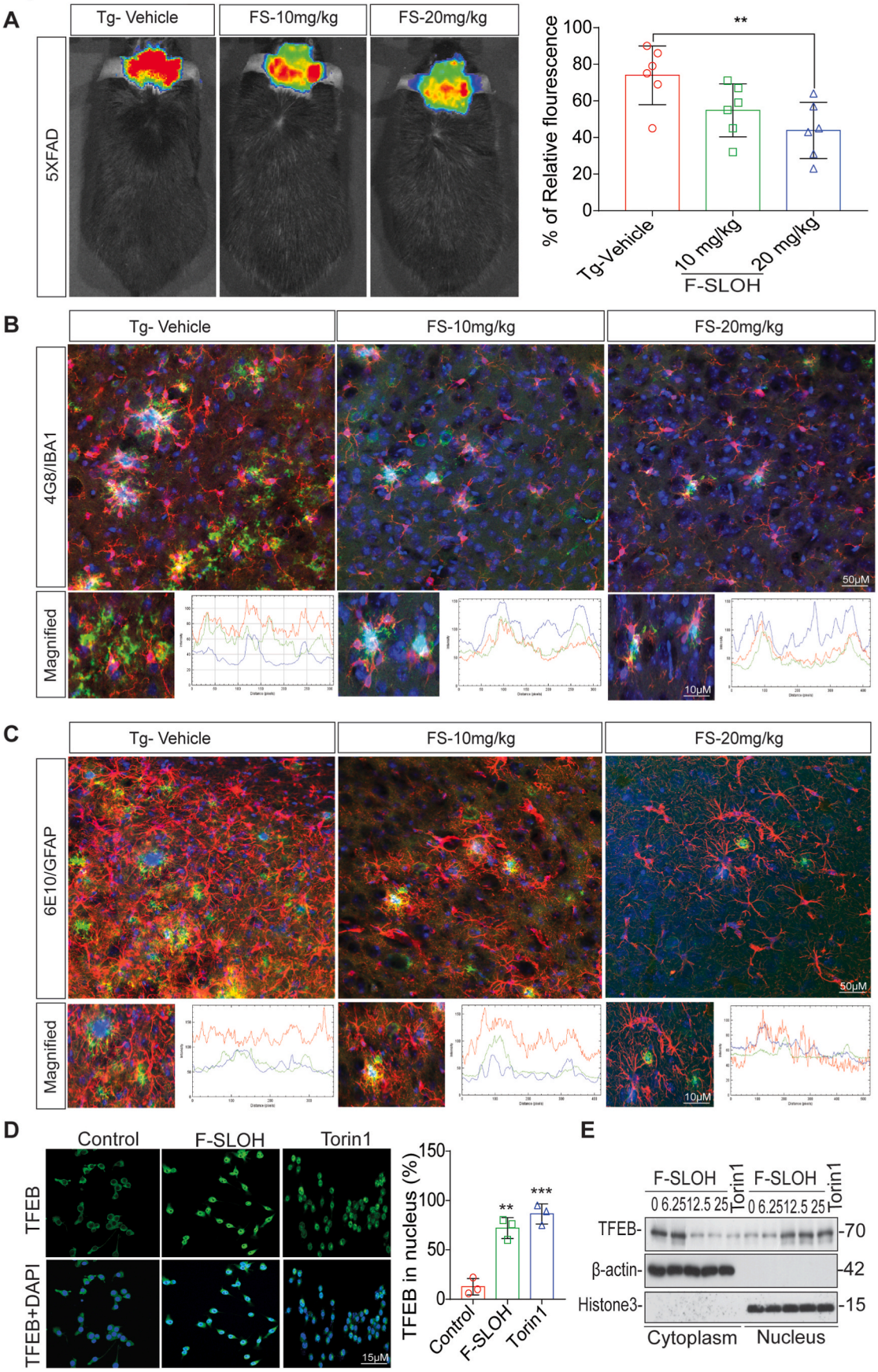

(caption on next page)

Fig. 6. Recruitment of microglia and astrocytes is required for the reduction of Aβ plaques in AD mouse models. (A) *In vivo* imaging of the animals to show the NIR fluorescence images of AD animals after the long-term treatment of F-SLOH and Tg-Vehicle and its quantification. (B) F-SLOH (10 and 20 mg/kg) treatment decreases 4G8 labelled Aβ plaque size and recruitment of Iba1 positive microglia in 5XFAD mice brain slice when compared to Tg-vehicle and its quantification. (C) F-SLOH (10 and 20 mg/kg) treatment decreases 6E10 labelled Aβ plaque size and recruitment of GFAP positive astrocytes in 5XFAD mice brain slice when compared to Tg-vehicle and its quantification. (D) F-SLOH (25 μM) or Torin 1 (250 nm) treatment in microglia cells for 24 h translocated TFEB in nucleus were stained and pictured in confocal microscope and its corresponding quantification. (E) F-SLOH (6.25,12.5 and 25 μM) or a positive control Torin 1 treatment in microglia cells at indicated concentrations for 24 h translocated the protein levels of cytosol TFEB to the nuclear TFEB shown in immunoblots.

full-length APP were significantly blocked (Fig. 4H and I) after BafA1 treatment at the indicated timepoint of CHX treatment in the AD cell model. Taken together, the above findings demonstrate that F-SLOH alleviates the proteolytic processing of APP and its metabolites by clearing immature APP *in vivo* and *in vitro* in AD models, implicating the induction of the degradation pathway.

3.5. F-SLOH mitigates tau pathology in 3XTg-AD mouse model

3XTg-AD mice show both Aβ and Tau pathologies, commonly these pathologies observed in this animal model are the same as those in humans. In the early months of age, the 3XTg-AD mice model starts with Aβ pathology and progression from 8th month, Tau pathology aggravates. So 3XTg-AD mice model is widely used for the therapeutic study. In 3XTg-AD mice, tau hyperphosphorylation and insoluble Tau deposition causes NFTs formation and thereby inducing the neurodegeneration in the brain. Hence, to determine the effect of F-SLOH on reducing the levels of phosphorylated Tau, we carried out a few experiments in the brain tissues of 3XTg-AD mice after F-SLOH treatment. To verify the levels of insoluble phospho Tau in the brain, we fractionated the brain tissue samples using Sarkosyl detergent extraction to separate the soluble and insoluble phospho Tau. Then, the F-SLOH treated brain tissue of 3XTg-AD mice were extracted using the sarkosyl detergent extraction and the protein samples were verified for soluble and insoluble phospho Tau. F-SLOH treatment predominantly reduced the insoluble phospho Tau (HT7, AT8, CP13, MC1 and PHF1) in the sarkosyl-insoluble fractions (Fig. 5A and B) of 3XTg-AD mice but not the sarkosyl-soluble Tau fractions, indicating that F-SLOH treatment particularly targets the insoluble phospho Tau for degradation. In addition, we verified the brain tissue slices for the AT8 and HT7 positive neuron load using immunohistochemistry. F-SLOH treatment reduced the AT8 and HT7 positive neuron load (Fig. 5C, D, 5E and 5F) in the brain tissue slices when compared to the Tg-Vehicle 3XTg-AD mice. Taken all together, the above findings demonstrate that F-SLOH mitigates tau pathology in 3XTg-AD mouse model, implicating the induction of the degradation of insoluble phospho Tau.

3.6. Recruitment of microglia and astrocytes is required for the reduction of Aβ plaques in AD mouse models

We have previously shown that F-SLOH is an effective and sensitive diagnostic probe for *in vivo* imaging of Aβ aggregates and plaques in AD mouse models in the early stage [17]. F-SLOH can not only target Aβ species but also effectively reduce Aβ monomers, oligomers as well as Aβ accumulation and deposition in AD mouse models. Therefore, we used F-SLOH as a monitoring diagnostic tool to detect Aβ accumulation and deposition in the animal brain after the completion of F-SLOH treatment regimen for AD prognosis. So, we did *in vivo* imaging of the animals to show the NIR fluorescence images of AD animals after the long-term treatment of F-SLOH and Tg-Vehicle and its quantification (Fig. 6A). Recent studies have demonstrated that microglia recruitment is involved in the Aβ clearance mechanism inducing autophagy lysosomal pathway in AD animal models. Thus, to verify the mechanism we detected the recruitment of microglia and astrocytes towards Aβ plaques and reduction of Aβ plaque size after F-SLOH treatment by inducing ALP. F-SLOH treatment dose-dependently reduced the Aβ plaque size and improved the recruitment of microglia and astrocytes towards the Aβ plaques (Fig. 6B and C). Transcription factor EB (TFEB) is the master regulator of autophagy and the autophagy lysosomal pathway (ALP) localized in the cytoplasm. Upon an activation, TFEB is dephosphorylated and then translocated to the nucleus where it promotes the expression of autophagy genes and lysosomal biogenesis [32]. Lysosomal and autophagic abnormalities are well-documented as the early neuropathological features of AD [33]. The recruitment of microglia and astrocytes towards the Aβ plaques may be involved in the Aβ clearance mechanism inducing autophagy lysosomal pathway in AD animal models. Thus, we cultured microglial cells to check ALP induction and TFEB nuclear translocation. Indeed, theranostic F-SLOH was found to activate TFEB and promote nuclear translocation of TFEB in cultured microglial cells (Fig. 6D and E). The results of both staining and immunoblotting when compared with the positive control, Torin1, an MTOR inhibitor and Trehalose, unambiguously demonstrated this effect.

3.7. F-SLOH activates transcription factor EB (TFEB) promoting autophagy and lysosomal biogenesis in cellular and animal models

In the AD brain, activation of the autophagy lysosomal pathway (ALP) has been shown to be useful for degrading toxic protein aggregates and damaged organelles [34]. To understand how APP-processed metabolites and Aβ are intracellularly cleared, we investigated whether F-SLOH could activate TFEB and induce ALP, which is highly impaired in AD progression. Firstly, F-SLOH treatment did not show any cytotoxicity and there was high cell viability in microglia cells, HT-22 cells (Supplementary Fig. S4I) and HeLa cells (Supplementary Figs. S4E and S4F) as demonstrated in MTT and LDH assays. Remarkably, the theranostic F-SLOH increased the number of the autolysosome displayed in electron micrograph indicating that F-SLOH treatment increased the lysosome number and autolysosome formation in comparison to the control and Torin1 (Fig. 7A and B). In addition, theranostic F-SLOH also activated TFEB and promoted its nuclear translocation in HT-22 cells and HeLa cells (Supplementary Figs. S5A, S5B, S5C, S5D, S5K and S5J) when compared with the positive controls Torin1 and Trehalose.

Furthermore, F-SLOH was found to dose-dependently increase LC3-II protein levels in both HT-22 (Fig. 7C) and HeLa cells (Supplementary Fig. S5E) revealing autophagy induction, without significant changes in P62 level in those cells (Supplementary Fig. S4C, S4D and S4G). We also determined whether F-SLOH could enhance autophagy flux in the presence or absence of the autophagosome lysosome fusion inhibitor chloroquine (CQ) and the lysosomal inhibitor bafilomycin A_1 (BafA1). Co-treatment of F-SLOH and autophagy inhibitors significantly increased the LC3-II protein level in both HT-22 cells (Fig. 7E) and HeLa cells (Supplementary Figs. S5F and S4H) compared to the inhibitors alone, indicating that both F-SLOH and Torin1 promote the formation of autophagosomes and fusion with lysosomes. To further confirm the above results, we employed stably over-expressed tf-LC3-cells to demonstrate the activation of autophagy flux. Similar to Torin1, F-SLOH significantly promoted autophagy flux and autophagosome lysosome fusion, but the fusion was blocked when the HT-22 (Fig. 7D) and HeLa cells (Supplementary Fig. S5G) were treated with CQ. As TFEB is also a master regulator in promoting lysosomal biogenesis, we examined whether F-SLOH could promote lysosomal biogenesis. We treated the cells with F-SLOH for 24 h and determined the lysosomal protein levels in the cell lysate. The results clearly demonstrated that F-SLOH significantly increased the LAMP1 and CTSD protein levels dose-dependently in HT-22 cells (Fig. 7F) and HeLa cells (Supplementary Fig. S5H). To

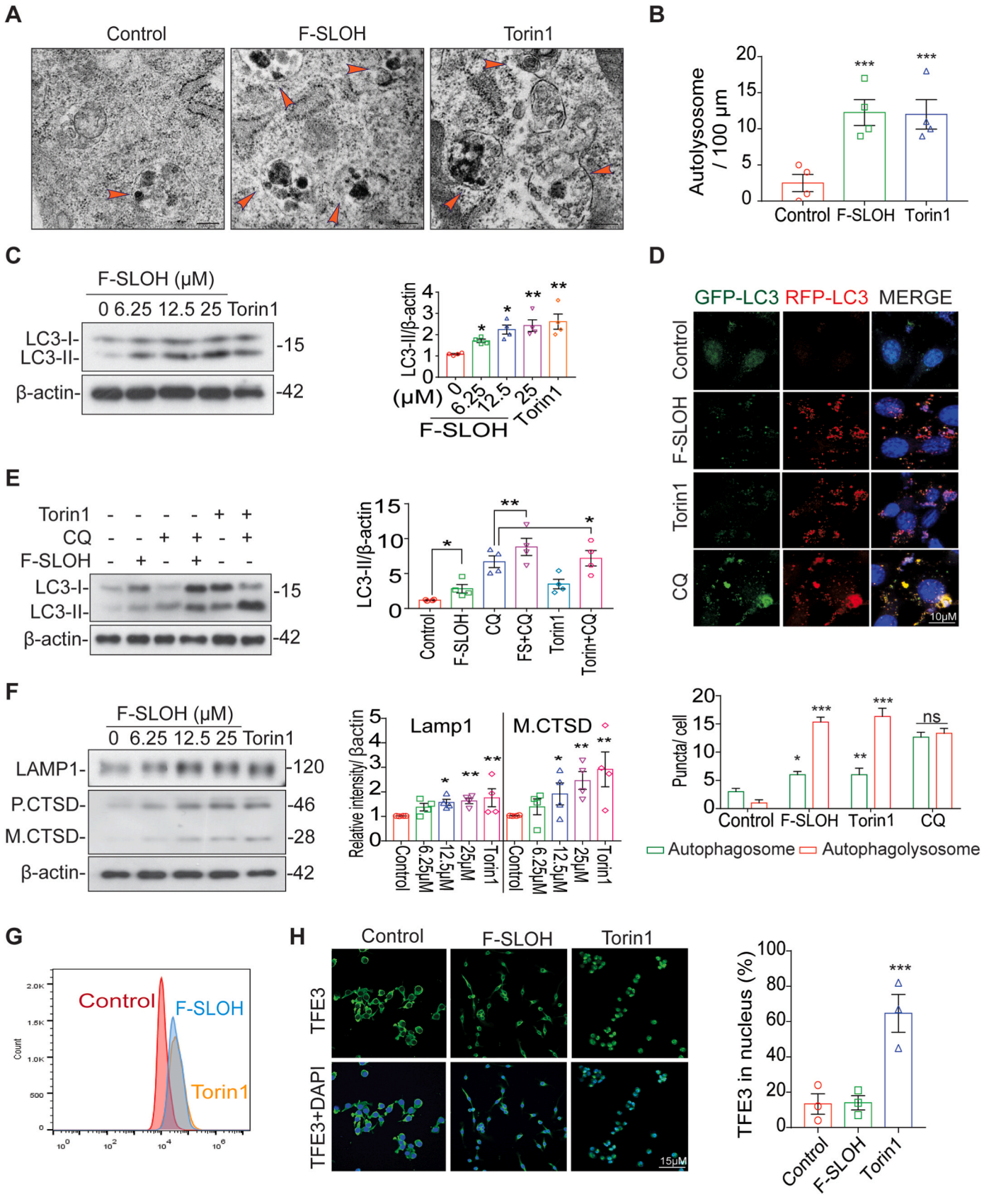

(caption on next page)

Fig. 7. F-SLOH activates transcription factor EB (TFEB) promoting autophagy and lysosomal biogenesis in cellular models. (A&B) The ultrastructure of the autolysosome displayed in electron micrograph indicates that F-SLOH treatment in the HT-22 cells increased the lysosome number and autolysosome formation in comparison to the control and Torin1. (C) HT-22 (6.25, 12.5 and 25 μM) cells were treated with F-SLOH or Torin1 for 24 h increased the protein expression levels of LC3B-II using western blotting and its corresponding quantification. (D) The HT-22 cells were transfected with stably expressing tf-LC3 plasmids for 48 h and then treated with F-SLOH (25 μM) for 24 h and compared with Torin 1 and the lysosomal inhibitor chloroquine (CQ)(20 μM). The stained cells were pictured using confocal microscope. The autolysosome and autophagosome puncta in the HT-22 cells were quantified accordingly. (E) F-SLOH and Torin1 were treated in HT-22 cells for 24 h in the presence or absence of CQ. F-SLOH treatment increased the protein expression levels of LC3B-II and its corresponding quantification. (F) F-SLOH treatment in HT-22 cells for 24 h increased the protein expression levels of LAMP1 and mature Cathepsin D in a dose-dependent manner and its corresponding quantification. (G) F-SLOH or Torin1 treatment in HT-22 cells for 24 h and the cells were incubated with LysoTracker Green DND-99 (75 nm) for 1 h. The stained cells were detected using flow cytometer and its quantified data is shown in figure. (H) F-SLOH (25 μM) or Torin1 treatment in microglial cells for 24 h were stained for TFE3 protein expression and pictured in confocal microscope and its corresponding quantification. (For interpretation of the references to colour in this figure legend, the reader is referred to the Web version of this article.)

further confirm the above results, we monitored the number of lysosomes with a Lysotracker probe using a flow cytometer. F-SLOH treatment significantly increased the number of lysosomes in the cells when compared to the control with reference to the positive control, Torin1, in HT-22 cells (Fig. 7G) and HeLa cells (Supplementary Fig. S5I). In addition, F-SLOH significantly increased the Lysotracker puncta in treated cells as visualised by the staining experiment in HT-22 cells (Supplementary Fig. S4K) and HeLa cells (Supplementary Fig. S4J and S4L). TFEB and TFE3 belong to the MiT family of microphthalmia-associated transcription factors (MITF), which are considered as master regulators of ALP. So, we investigated whether theranostic F-SLOH can activate TFE3 and translocate TFE3 in microglial cells. Surprisingly, theranostic F-SLOH did not activate TFE3 but translocated TFEB into the nucleus of microglial cells (Fig. 7H). From this experiment, it was clearly shown that theranostic F-SLOH activated only TFEB but did not activate other MITF members.

To find out whether F-SLOH could promote autophagy and ALP *in vivo, WT* (C57BL/6) mice were treated with F-SLOH for one week. Body weight of the mice did not notably change after the treatment (Supplementary Figs. S6A and S6B). Remarkably, F-SLOH increased the levels of LAMP1, mature CTSD and LC3B-II in the WT mice (Supplementary Fig. S6C) indicating the *in vivo* efficacy of F-SLOH in promoting ALP. MTORC1 is one of the major kinases that phosphorylates TFEB and localizes into the cytoplasm; therefore, activation of TFEB depends on its dephosphorylation. MTORC1 inhibition may lead to the dephosphorylation of TFEB, activating its nuclear translocation [23]. To our surprise, F-SLOH did not inhibit MTORC1 but dose-dependently translocated TFEB into the nucleus, independent of MTORC1 and its downstream kinase inhibition (Supplementary Fig. S6D). Collectively, we have unambiguously demonstrated that F-SLOH activates the autophagy-lysosome pathway effectively for degrading toxic protein aggregates of Aβ *in vitro* and *in vivo*. F-SLOH treatment increases the levels of LC3B-II, mature CTSD and LAMP1 without influencing the levels of MTORC1 substrates in brain of WT mice.

3.8. TFEB is essential for F-SLOH-induced autophagy activation and lysosomal biogenesis

To determine whether TFEB is required for F-SLOH-induced autophagy and lysosomal biogenesis activation, we knocked down TFEB and looked for F-SLOH-induced activation of autophagy and lysosomal genes in cells. Interestingly, we found that the F-SLOH-induced promotion of autophagy and lysosomal biogenesis was dependent of TFEB activation (Figs. S7A and S7B). Furthermore, F-SLOH treatment increased the expression levels of LC3B-II, LAMP1, and CTSD in the presence or absence of CQ in TFEB WT cells (Fig. 8A and B). However, there were no changes in the TFEB Knock Out (KO) cells, demonstrating that TFEB is important for F-SLOH to induce activation of autophagy and lysosomal biogenesis. We further corroborated our findings in both HT-22 and HeLa cell lines in TFEB knockdown condition. Effective knockdown of TFEB significantly abolished the ability of F-SLOH to increase LC3B-II expression (Supplementary Fig. S8A) in both HT-22 cells and HeLa cells in the presence or absence of CQ (Supplementary Figs. S7C and S7D). Meanwhile, TFEB knockdown significantly obliterated the ability of F-SLOH to induce an increase in LAMP1 and CTSD levels in both of the cell models (Supplementary Figs. S8B and S8C). Such a knockdown also significantly eliminated the F-SLOH effect of increasing the lysotracker number in those cells (Supplementary Fig. S7E). Taken together, these results provides convincing evidence that TFEB is essential for F-SLOHto induce autophagy and lysosomal biogenesis *in vitro* and *in vivo*.

3.9. MAPK1 and PP2A, not MTOR and its substrates, is essential for F-SLOH-induced activation of TFEB and autophagy lysosomal biogenesis

TFEB is phosphorylated at multiple sites when docked in the cytoplasm. Various kinases are involved in phosphorylating TFEB, including MTORC1, MAPK1, GSK3β and AKT [35]. To examine the kinases involved in dephosphorylation of TFEB for the translocation of TFEB into the nucleus induced by F-SLOH, six inhibitors, namely: SB216763, GSK-3β inhibitor; FK506 and CsA (Cyclosporin A), calcineurin inhibitors; TG (thapsigargin) endoplasmic reticulum calcium inhibitor; and BAPTA-AM, a calcium chelator were employed in these studies. As clearly shown in Supplementary Figs. S8D, S8E, S8F and S8G, none of the inhibitors abolished the ability of F-SLOHto induce TFEB translocation in cells. We then determined the site of TFEB dephosphorylation in F-SLOH-induced translocation in cell models. As shown in Fig. 8C and D, F-SLOH treatment dose-dependently and time-dependently reduced phospho-TFEB (S142) and induced nuclear translocation of TFEB in HT-22 and HeLa cells (Supplementary Figs. S9A and S9B). To further confirm the F-SLOH mediated activation of TFEB, we transiently transfected WT cells with mutant TFEB (S142D) plasmids. F-SLOH-induced TFEB activation was found to be abolished in TFEB (S142D)-overexpressed cells, indicating S142 phosphorylation site is essential for the F-SLOH-induced activation of TFEB and its concomitant nuclear accumulation (Fig. 8F). Furthermore, the mutant TFEB overexpressed cells abolished the increase in the lysotracker number even after F-SLOH treatment (Fig. 8E). These findings were further confirmed by Western blot, wherein the mutant TFEB overexpressed cells did not show increase in the expression levels of proteins LC3B-II, LAMP1 and CTSD (Fig. 8G). Meanwhile, TFEB knockdown significantly blocked the F-SLOH-mediated decrease in p-TFEB, along with the molecular weight shift, as revealed by the Western blot results (Supplementary Fig. S9M and S9N). As TFEB dephosphorylation is an important event during activation of TFEB and translocation to nucleus, we checked whether F-SLOH-induced TFEB activation and TFEB dephosphorylation is mediated with the help of phosphatases like calcineurin, PP2A or PP3A. So, we used different inhibitors of phosphatases including FK506, CsA (Cyclosporin A), and Okadaic acid (OA) to investigate F-SLOH-induced TFEB translocation. Calcineurin inhibitor (Supplementary Fig. S8E) did not abolish the ability of F-SLOH to induce TFEB translocation in cells but the PP2A inhibitor, OA blocked the F-SLOH-induced TFEB translocation into nucleus (Fig. 8H), indicating that PP2A induced dephosphorylation is essential for the F-SLOH-induced activation of TFEB and its subsequent nuclear accumulation. As shown in the results of both staining and immunoblotting, when compared with those of the control and F-SLOH-treated one in the presence or absence of OA (Fig. 8I and J),

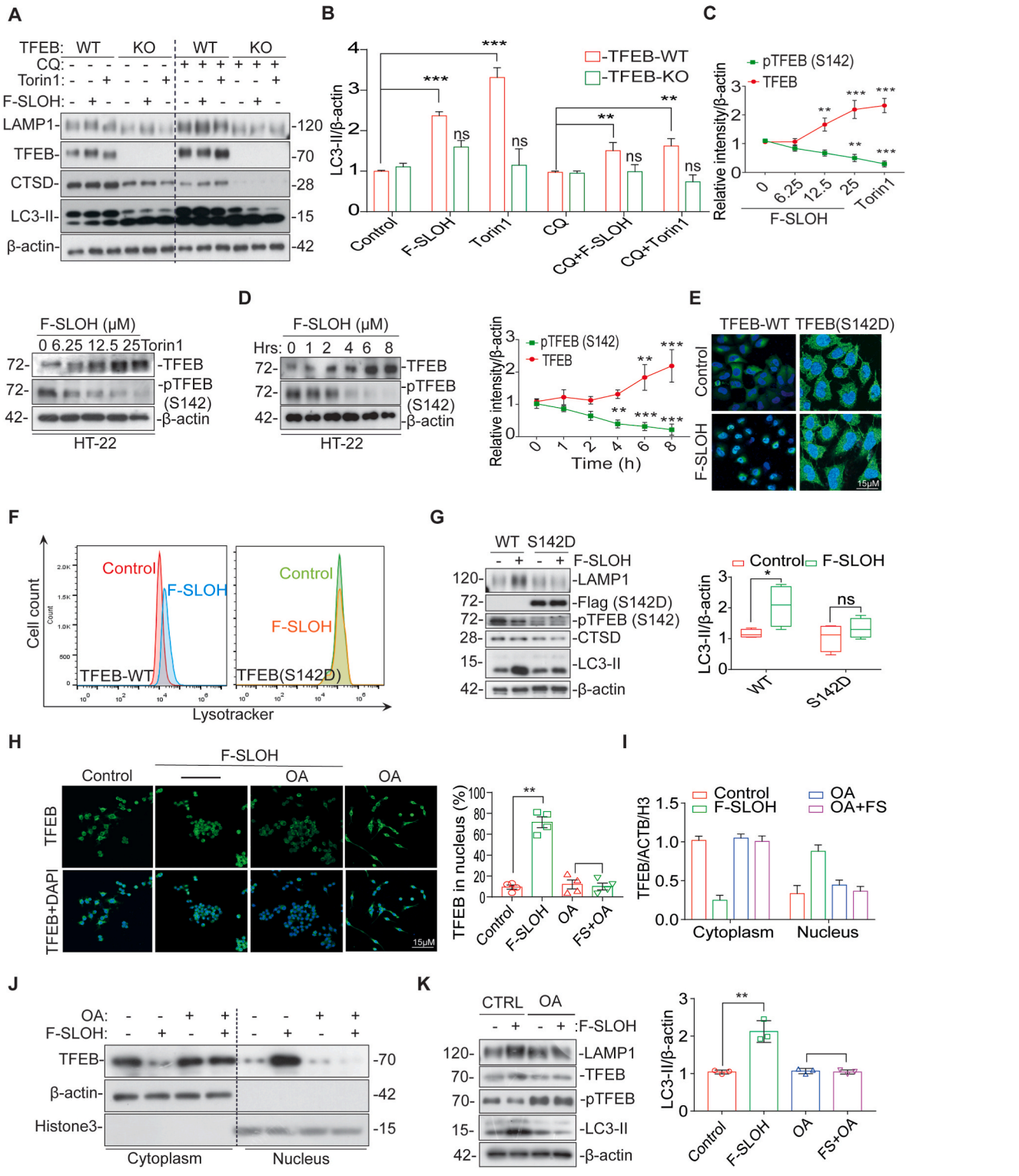

(caption on next page)

Fig. 8. TFEB is essential for F-SLOH-induced autophagy activation and lysosomal biogenesis. (A) Wild type HeLa and TFEB knockout (KO) cells were treated with F-SLOH (25 μM) Torin1 (250 nM) for 24 h in the presence or absence of CQ (20 μM). The blots show the protein expression levels of LC3B-II and (B) its corresponding quantification. (C) In HT-22 cells different concentrations of F-SLOH (6.25,12.5,25 μM) or 25 μM of F-SLOH (D) at different durations (0–8 h). There was pronounced gel-shift of endogenous TFEB indicating that F-SLOH caused TFEB dephosphorylation and reduced pTFEB (S142) in both dose- and time-dependent manner. (E) TFEB (WT) or TFEB (S142D) mutant plasmid were transfected in HT-22 cells and treated with F-SLOH (25 μM) for 24h, cells were incubated with LysoTracker Green DND-99 (50 nm) for 1h to assess lysotracker positive cells. F-SLOH increased the lysosome contents in TFEB (WT) and blocked the increase of lysosome in the TFEB (S142D) mutant HT-22 cells as detected by flow cytometer. (F) F-SLOH treatment in HeLa cells were transfected with TFEB (S142D) mutant plasmid blocking the nuclear translocation of TFEB. The pictures depict the number of cells with nuclear TFEB and the mutant-blocked cells with TFEB staining were quantified. (G) F-SLOH treatment for 24 h in HT-22 cells transfected with TFEB (WT) or TFEB (S142D) mutant plasmid were assessed for the protein expression levels of autophagy markers. TFEB (S142D) mutant blocked the increase of F-SLOH-induced protein expression levels of autophagy markers namely LAMP1, CTSD and LC3B-II as compared to the TFEB (WT) counterparts. (H) Okadaic acid (OA) blocked the endogenous TFEB translocation into the nucleus on treatment with F-SLOH (25 μM). Pre-treatment of microglial cells with OA for 30 min followed by F-SLOH treatment to the cells for another 24h, the nuclear translocation of TFEB were detected by confocal microscopy. (I&J) OA blocked the F-SLOH induced TFEB translocation in microglia cells at indicated concentrations for 24 h as shown in immunoblots. (K) OA blocked the increase of F-SLOH-induced protein expression levels of autophagy markers namely LAMP1, TFEB and LC3B-II in microglial cells. Each data point represents the average of three replicates and represented as mean ± SEM. (For interpretation of the references to colour in this figure legend, the reader is referred to the Web version of this article.)

they are clearly demonstrated the F-SLOH effect and indicated the PP2A induced dephosphorylation is indispensable. These findings were further confirmed by the Western blot, in that the OA treated cells with F-SLOH did not show increase in the expression levels of proteins LC3B-II, LAMP1 and TFEB (Fig. 8K) and blocked the decrease of pTFEB. Taken all together, these results constitute convincing evidence that PP2A is essential for F-SLOH to induce TFEB nuclear translocation and autophagy lysosomal biogenesis *in vitro* and *in vivo*.

It is well-known that MTORC1 and its substrates are essential for the regulation of TFEB nuclear accumulation [35]. Thus, we examined whether F-SLOH would inhibit MTORC1 and promote the translocation of TFEB. Intriguingly, F-SLOH did not inhibit or depend on MTORC1 and its downstream targets for the nuclear translocation of TFEB in HT-22 cells (Fig. 9A) and HeLa cells (Supplementary Fig. S9E) as confirmed by immunoprecipitation (Supplementary Fig. S9F). In addition, F-SLOH did not inhibit or affect other kinases including GSK3β (Supplementary Fig. S9G), and AKT (Supplementary Figs. S9H and S9I) in a dose- and time-dependent manner. These results further verified that the F-SLOH-mediated TFEB activation or increase in the expression of ALP markers (LC3B-II, LAMP1, CTSD) were not affected in the presence of GSK3β/AKT inhibitors (Supplementary Figs. S9J and S9K and S9L).

MAPK1/ERK2, an endogenous kinase, has been known to phosphorylate TFEB at S142 site and inhibits the translocation of TFEB into a nucleus [23,35,36]. F-SLOH treatment indeed inhibited the protein expression of MAPK1/ERK2 in a dose- and time-dependent manner in HT-22 cells (Fig. 9B and C) and HeLa cells (Supplementary Figs. S9C and S9D). Further, we determined whether MAPK1/ERK2 inhibition is necessary for the F-SLOH-induced activation of TFEB. HT-22 cells were transiently transfected with WT-ERK plasmids to overexpress MAPK1/ERK2. F-SLOH induced activation of TFEB, and nuclear accumulation of TFEB (Fig. 9D) was blocked by the overexpression of MAPK1/ERK2, indicating that inhibition of MAPK1/ERK2 is essential for the F-SLOH-induced activation of TFEB. Similar results were observed in lysotracker staining (Fig. 9E) and Western blot experiments (Fig. 9F). Immunostaining also showed that the MAPK1/ERK2 activator, doxycycline, attenuated the F-SLOH-induced activation of TFEB and nuclear accumulation of TFEB in the cells (Fig. 9G). The results of lysotracker intensity (Fig. 9H) and Western blot (Fig. 9I) investigations also indicated that doxycycline abolished the F-SLOH effect. The above results collectively demonstrated that inhibition of MAPK1/ERK2 is essential for F-SLOH to promote autophagy and lysosomal biogenesis via TFEB dephosphorylation and nuclear accumulation, *in vitro* and *in vivo*.

3.10. TFEB is essential for F-SLOH induced degradation of APP metabolites, phospho Tau and Aβ in vitro and in vivo in AD models

Recent studies have demonstrated that molecules targeting TFEB activation can promote the degradation of APP metabolites, phospho tau and Aβ aggregates [23,37]. Interestingly, F-SLOH treatment promoted autophagy and lysosomal biogenesis in brain homogenates of both 3XTg-AD and 5XFAD mice as revealed by the immunoblot assays. F-SLOH induced the activation of TFEB and increased the expression levels of LC3B-II, LAMP1 and CTSD in the brains of 5XFAD (Fig. 10A) and 3XTg-AD (Fig. 10B) mice. Furthermore, F-SLOH-induced activation of TFEB was independent of MTORC1 and its downstream signalling in both 5XFAD (Supplementary Figs. S10A) and 3XTg-AD mice (Supplementary Fig. S10B). The expression levels of proteins pMTOR, pP70S6K and p4EBP1 were found in brain homogenate fractions as revealed by the immunoblot assays. Interestingly, we also observed nuclear translocation of TFEB in brains of WT mice treated with F-SLOH (Fig. 10C). Similarly, F-SLOH treatment increased the lysosome and autolysosome formation in the brains of 5XFAD mice (Fig. 10D). The ultrastructure of the hippocampus as seen in electron micrographs indicated that F-SLOH treatment enhanced the autolysosome formation as compared to the Tg-vehicle treatment. Moreover, to determine whether F-SLOH could induce lysosome-mediated degradation of APP, phospho Tau, Aβ and its metabolites, CQ, an autophagy inhibitor was employed. As expected, in N2a cells stably overexpressing APP695 and Tau-P301L mutations, F-SLOH + CQ treatment significantly blocked the degradation of APP and CTFs, compared to F-SLOH alone treatment (Supplementary Fig. S10C S10E and S10G). Meanwhile, LC3B-II expression levels were further increased in the presence of CQ and F-SLOH treatment. In addition, F-SLOH treatment in the TFEB knockdown N2a cells (overexpressing APP695 and Tau-P301L mutations) significantly abolished the degradation of APP, phospho Tau and CTFs (Supplementary Figs. S10D and S10F) clearly stating that TFEB is important for the degradation of Tau and APP metabolites. Taken together, the above results evidently indicated that F-SLOH treatment induced the lysosomal degradation of APP metabolites and tau aggregates via TFEB activation *in vitro* and *in vivo* in AD models (Fig. 11).

4. Discussion

For the first time, we have demonstrated that F-SLOH can degrade Aβ aggregates, Aβ oligomers, phospho Tau, APP and its metabolites via TFEB activation *in vitro* and *in vivo* in AD models by promoting autophagy lysosomal signalling pathway. Over the past years, mounting evidence has suggested that Aβ specific targeting and clearance would be beneficial for effective clinical approach of treating AD [32]. Several studies have demonstrated Aβ targeting drugs, which merely inhibit aggregate or oligomer formation, are not an effective disease-modifying treatment for AD [38]. Given the multifactorial nature of AD, it is hypothesized that a drug with multiple treatment/targeting properties such as inhibition of Aβ aggregation, degradation of Aβ species and APP metabolites, alleviation of neuro-inflammation, attenuation of synaptic deficits, and amelioration of cognitive impairment, would be more likely to provide an effective treatment. F-SLOH has been developed as a theranostic agent which can detect the cerebral aggregated Aβ in early

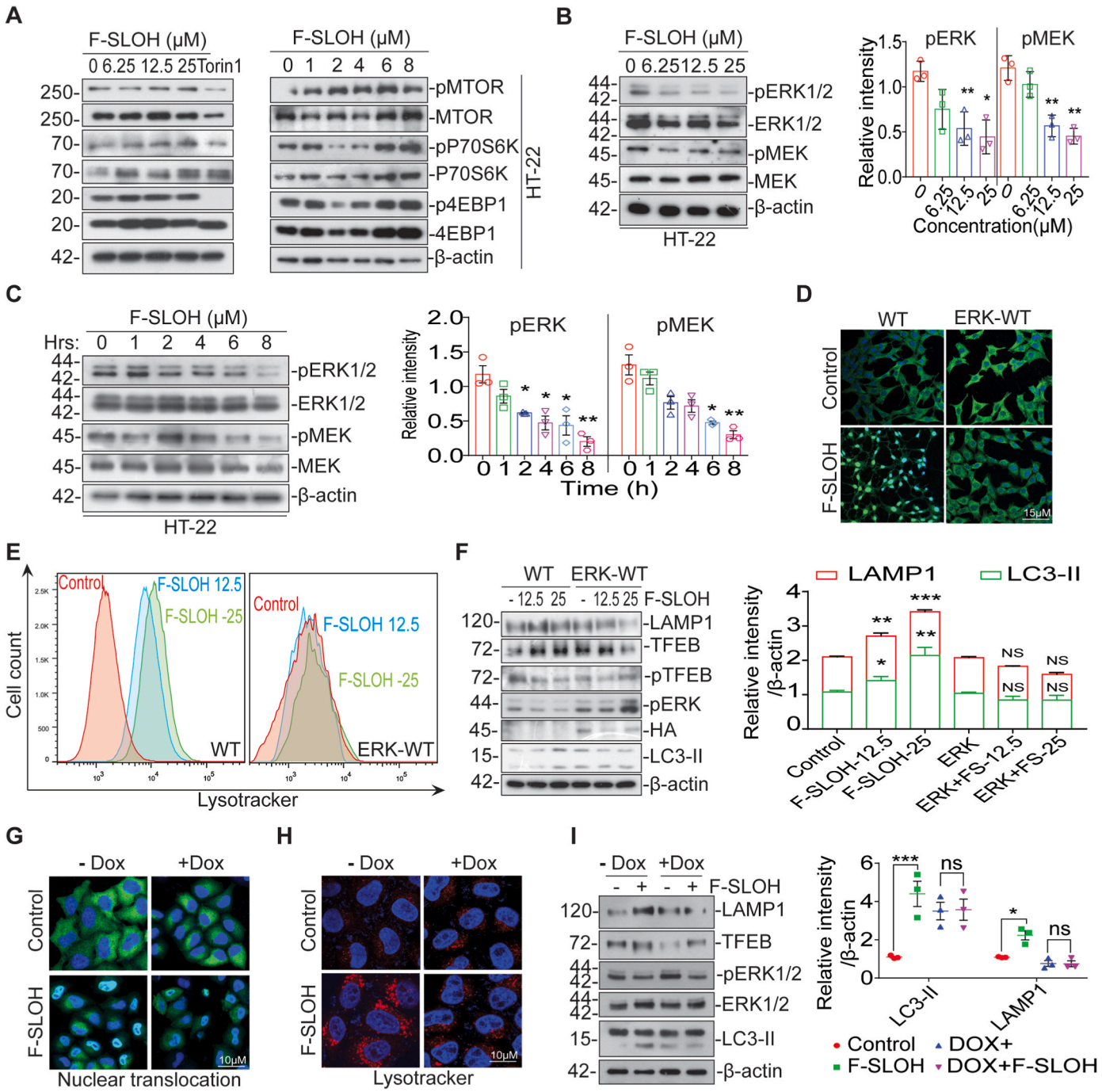

Fig. 9. MAPK1 is essential for F-SLOH-induced activation of TFEB and autophagy lysosomal biogenesis rather than MTOR and its substrates. (A) F-SLOH treatment did not inhibit the MTOR signalling pathway and F-SLOH dephosphorylated TFEB independent of MTOR pathway. F-SLOH treatment in HT-22 cells for 24 h or F-SLOH treatment at different time points did not inhibit the protein expression levels of p-MTOR, p-P70S6K and p-4EBP1 as shown by immunoblots. (B) In HT-22 cells, different concentrations of F-SLOH (6.25, 12.5 and 25 μM) or 25 μM of F-SLOH at various time points (0–8 h). (C) There was a clear inhibition of MAPK kinases namely pERK1/2 and pMEK which triggered TFEB dephosphorylation at the S142 site of TFEB in both dose- and time-dependent manner. (D) HT-22 cells were transfected with WT or ERK-WT plasmid and treated with F-SLOH (25 μM). ERK overexpression blocked the F-SLOH-activated TFEB translocation. The pictures depict the immunostaining of TFEB translocation in nucleus and its corresponding quantification. (E) HT-22 cells were transfected with WT or ERK-WT plasmid and treated with F-SLOH (25 μM) for 24 h. F-SLOH induced the increase in lysosome contents in WT cells and the ERK-WT overexpression blocked the increase of lysosome in HT-22 cells. The treated cells were incubated with LysoTracker Green (50 nm) for 1 h as shown by flow cytometry. (F) HT-22 cells were transfected with WT or ERK-WT plasmid and were treated with F-SLOH (12.5 and 25 μM) for 24 h and assessed for the protein expression levels of autophagy markers. F-SLOH treatment in ERK-WT overexpressed cells blocked the increase in protein expression levels of CTSD, LAMP1 and LC3B-II as compared to the WT and quantified accordingly. (G) Cells were treated with F-SLOH in the absence or presence of Doxycycline. Doxycycline treatment blocked the F-SLOH activated TFEB translocation in the cells as shown in the pictures using immunostaining and the nuclear translocation of TFEB was quantified. (H) Doxycycline blocked the increase of lysosome in the F-SLOH treated cells incubated with LysoTracker Green (50 nm) for 1 h and was detected using flow cytometry. (I) Doxycycline pre-treatment in cells blocked the F-SLOH-induced increase of protein expression levels of LAMP1, CTSD and LC3B-II when compared to the absence of Doxycycline in cells using Western blot analysis and its corresponding quantification. Each data represents the average of three replicates and data represented as mean ± SEM. (For interpretation of the references to colour in this figure legend, the reader is referred to the Web version of this article.)

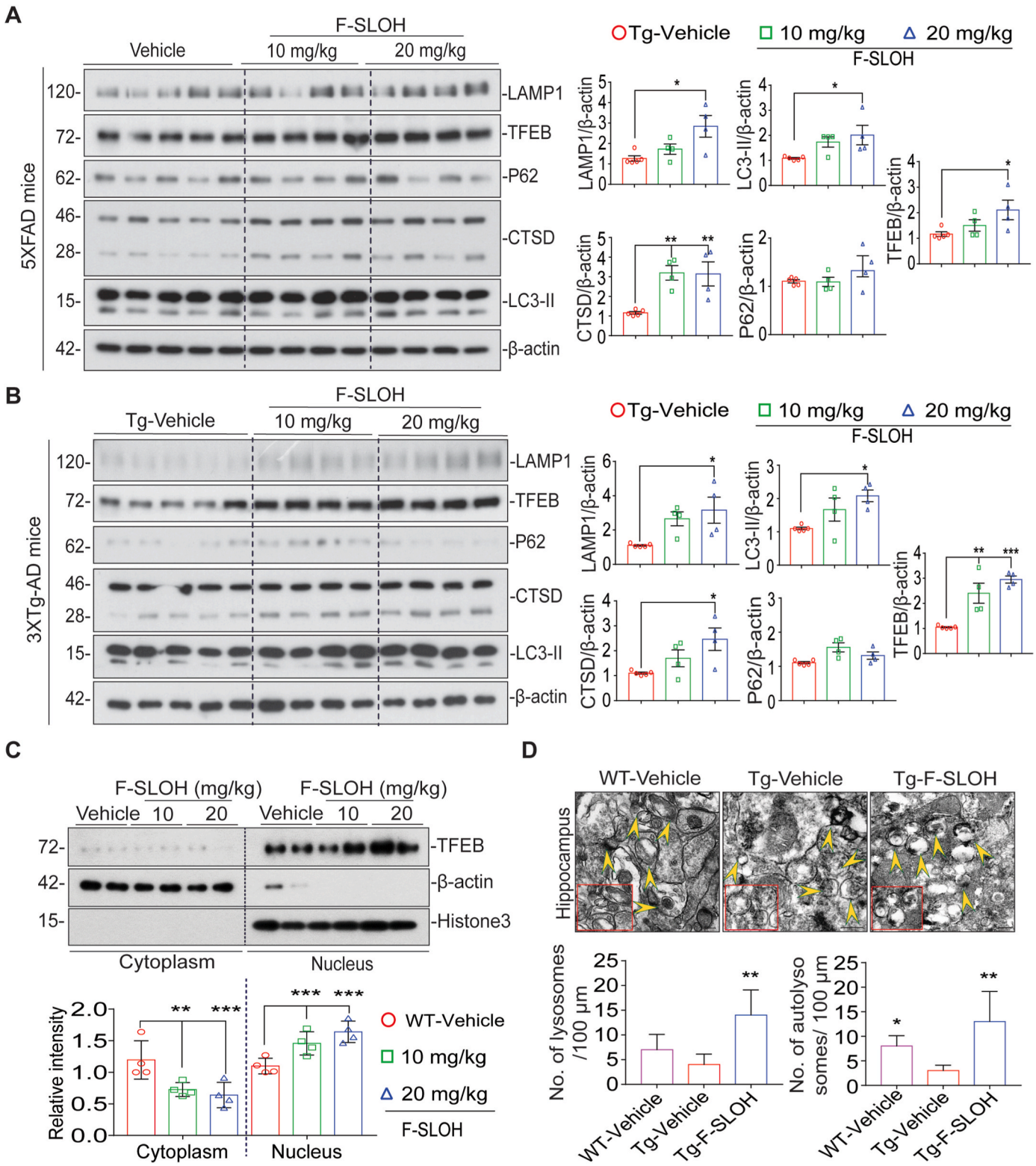

Fig. 10. TFEB is essential for F-SLOH induced degradation of APP metabolites and Aβ *in vitro* and *in vivo* in AD models. (A) F-SLOH activates TFEB to promote autophagy and autophagy lysosomal pathway in 5XFAD mice. The immunoblots indicate the protein expression levels of LAMP1, CTSD, TFEB, P62 and LC3B-II and its corresponding quantification representing treatment effects of F-SLOH (10 and 20 mg/kg) in the whole brain lysate of 5XFAD mice. (B) F-SLOH activates TFEB to promote autophagy and autophagy lysosomal pathway in 3XTg-AD mice. The immunoblots indicate the protein expression levels of LAMP1, CTSD, TFEB, P62 and LC3B-II and its quantification corresponding to the treatment effects of F-SLOH (10 and 20 mg/kg) in brain lysates of 3XTg-AD mice. (C) The immunoblots indicate the protein expression levels of cytoplasmic TFEB and nuclear TFEB as compared to the ratio of β-actin and Histone 3 and its corresponding quantification representing treatment effects of F-SLOH (10 and 20 mg/kg) in the whole brain lysate of C57BL/6 mice. (D) F-SLOH treatment increased the lysosome and autolysosome formation in the brain slice in 5XFAD mice. The ultrastructure of the hippocampus displayed in electron micrograph indicated that F-SLOH treatment increased the autolysosome formation when compared to the vehicle treated Tg group. Quantification of number of lysosome and autolysosome in the brain slice of 5XFAD mice.

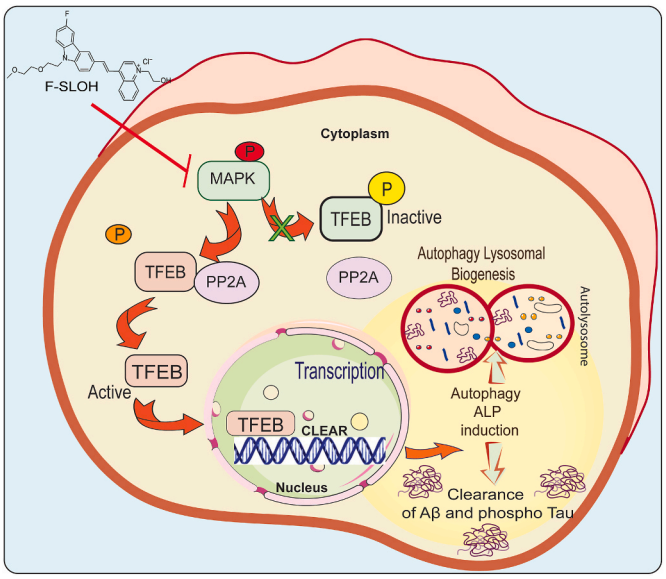

Fig. 11. Schematic diagram indicates the mechanism of F-SLOH via activating TFEB and promoting autophagy lysosomal pathway.
Schematic illustration of the mechanism of F-SLOH treatment via activation of TFEB resulting in promotion of autophagy lysosomal pathway *in vitro* and *in vivo*. Inhibition of MAPK and activation of PP2A is essential for F-SLOH-induced TFEB dephosphorylation for nuclear translocation to promote autophagy and lysosomal biogenesis in clearance of Aβ.

stage of disease progression; it is biocompatible, non-cytotoxic, readily BBB-permeable and cleared rapidly in an AD mouse model [15,17]. In the present study, we have shown that F-SLOH is highly bioavailable in the brain. It can directly bind to aggregated Aβ and inhibit the formation of both Aβ oligomers and Aβ plaques in the brains of 3XTg-AD and 5XFAD mice. Furthermore, F-SLOH treatment not only significantly decreased the Aβ deposits in 3XTg-AD and 5XFAD mice models but also significantly improved learning and spatial memory, alleviated neuro-inflammation and mitigated synaptic deficits in preclinical AD animal models. These results imply that F-SLOH is a multi-targeted agent which could be effective in the early stages of AD.

Studies have shown that autophagy and ALP deteriorate in the early stages of AD [34,39] leading to the accumulation of APP metabolites, phospho Tau and Aβ deposits [31,34]. Meanwhile, recent studies have demonstrated that TFEB is a master regulator and driver of the autophagy machinery, promoting ALP in disease conditions [36,37]. Therefore, TFEB is an important therapeutic target for promoting ALP for the clearance of accumulated APP metabolites, phospho Tau and Aβ deposits in attenuating AD pathology in early stage of disease conditions [23,37]. Remarkably, we have demonstrated that F-SLOH significantly activates TFEB through MAPK1/PP2A pathway and promotes ALP effectively for degrading toxic protein Aβ aggregates *in vitro* and *in vivo* in AD models (Fig. 11). Additionally, F-SLOH inhibits MAPK1/ERK2 activity and enhance PP2A function to dephosphorylate TFEB. Further, the activated TFEB can translocate and accumulate in the nucleus, thereby promoting the autophagy and lysosomal biogenesis for the degradation of accumulated APP metabolites and phospho Tau in the brains of AD models.

In conclusion, the current study represents the first *in vivo* evidence that the theranostic agent, F-SLOH has multiple effective etiology-targeting capabilities to treat/mitigate multiple neuropathological abnormalities in AD mouse models. F-SLOH ameliorates Aβ pathologies by decreasing the levels of toxic Aβ oligomers and APP metabolites by activating TFEB and promoting ALP. The findings of this study could lead to important advancements in AD drug development.

Authors' Contributions

The research study was conceived and conceptualized by: ML, MSW, HWL, AI. Methodology: AI, SKK, XW, VK, SGS, BCKT, ZZ, CFS, JL, SSKD. Investigation: AI, SKK, XW, VK, SGS, ZZ, CFS, JL, SSKD. Data curation: AI, SKK, XW, VK, BCKT, MSW, HWL, ML, JXS, SSKD, JHL. Writing original draft: AI, SKK, HWL, MSW and ML. Writing review and editing: ML, JXS, JHL, SSKD, MSW, BCKT, JQT and KHC. Funding acquisition: ML, MSW, HWL, AI. Resources: ML, MSW, HWL. All authors read and approved the final manuscript.

Funding

This present study was funded and supported by the grants of Research Grants Council of Hong Kong Collaborative Research Fund (C2012-15G), the General Research Fund (GRF/HKBU12101417, GRF/HKBU12100618) and Health and Medical Research Fund (HMRF/17182541, HMRF/17182551) from Hong Kong Government, and research grants from Hong Kong Baptist University (HKBU/RC-IRCs/17–18/03, IRCMS/19–20/H02), also was supported by the National Natural Science Foundation of China (NSFC 81703487, NSFC 81773926) and Shenzhen Science and Technology Innovation Commission (JCYJ20180302174028790, JCYJ20180507184656626).

Ethics statement and approval

All animal experiments were approved by the Hong Kong Baptist University Committee on the Use of Human and Animal Subjects in Teaching and Research (HASC approval #HASC/17–18). All animal experiments were performed in accordance with the relevant guidelines and regulations of HASC. The researchers who performed all the experiments got approval from the Department of Health for performing the animal experiments in Hong Kong under the licence (20–26) in DH/HT&A/8/2/6 Pt.1.

Data availability statement

All data generated or analysed during this study are included in the manuscript. The data supporting this article will be made available by the authors, without undue reservation to any qualified researcher. Data will be made available on request to the corresponding author Prof. Min Li upon reasonable request.

Declaration of competing interest

The authors declare that they do not have any known competing financial interests and that personal relationships did not influence the research work reported in this manuscript.

Acknowledgements

We thank Prof. Richard J. Youle (National Institute of Neurological Disorders and Stroke, Bethesda, USA) and Prof. Myung-Shik Lee (Yonsei University College of Medicine, Seoul, Republic of Korea) for their kind gift of Wild type HeLa cells and TFEB knock out HeLa cells. We thank Prof. Andrea Ballabio (Professor of Medical Genetics, Department of Translational Medicine, University of Naples, Italy) for his kind gift of S142D plasmid. We thank Dr. Roy Chun-Laam Ng (Research Assistant Professor, Department of Medicine, HKU) and Dr. Wong H. M. Karen (HKU QMH Electron Microscope Unit Queen Mary Hospital, Hong Kong) for their help in TEM imaging. We thank Dr. Carol Chu for her enormous support in ordering reagents and managing our lab needs. We also thank Dr. Martha Dahlen for her English editing of this manuscript.

Appendix A. Supplementary data

Supplementary data to this article can be found online at https://doi.org/10.1016/j.redox.2022.102280.

References

[1] J. Hardy, A hundred years of Alzheimer's disease research, Neuron 52 (2006) 3–13.
[2] A. Alzheimer's, 2016 Alzheimer's disease facts and figures, Alzheimers Dement 12 (2016) 459–509.
[3] R. Brookmeyer, E. Johnson, K. Ziegler-Graham, H.M. Arrighi, Forecasting the global burden of Alzheimer's disease, Alzheimers Dement 3 (2007) 186–191.
[4] 2020 Alzheimer's disease facts and figures, Alzheimers Dement (2020).
[5] R. Sengoku, Aging and Alzheimer's disease pathology, Neuropathology 40 (2020) 22–29.
[6] S. Li, D.J. Selkoe, A mechanistic hypothesis for the impairment of synaptic plasticity by soluble Abeta oligomers from Alzheimer's brain, J. Neurochem. 154 (2020) 583–597.
[7] M. Guglielmotto, D. Monteleone, A. Piras, V. Valsecchi, M. Tropiano, S. Ariano, M. Fornaro, A. Vercelli, J. Puyal, O. Arancio, M. Tabaton, E. Tamagno, Abeta1-42 monomers or oligomers have different effects on autophagy and apoptosis, Autophagy 10 (2014) 1827–1843.
[8] N. Katzmarski, S. Ziegler-Waldkirch, N. Scheffler, C. Witt, C. Abou-Ajram, B. Nuscher, M. Prinz, C. Haass, M. Meyer-Luehmann, Abeta oligomers trigger and accelerate Abeta seeding, Brain Pathol. 30 (2020) 36–45.
[9] D.J. Selkoe, J. Hardy, The amyloid hypothesis of Alzheimer's disease at 25 years, EMBO Mol. Med. 8 (2016) 595–608.
[10] J. Sevigny, P. Chiao, T. Bussiere, P.H. Weinreb, L. Williams, M. Maier, R. Dunstan, S. Salloway, T. Chen, Y. Ling, J. O'Gorman, F. Qian, M. Arastu, M. Li, S. Chollate, M.S. Brennan, O. Quintero-Monzon, R.H. Scannevin, H.M. Arnold, T. Engber, K. Rhodes, J. Ferrero, Y. Hang, A. Mikulskis, J. Grimm, C. Hock, R.M. Nitsch, A. Sandrock, The antibody aducanumab reduces Abeta plaques in Alzheimer's disease, Nature 537 (2016) 50–56.
[11] O. Antonoglou, K. Giannousi, S. Mourdikoudis, C. Dendrinou-Samara, Magnetic nanoemulsions as candidates for Alzheimer's disease dual imaging theranostics, Nanotechnology 31 (2020) 465702.
[12] M.L. Bolognesi, A. Gandini, F. Prati, E. Uliassi, From companion diagnostics to theranostics: a new Avenue for Alzheimer's disease? J. Med. Chem. 59 (2016) 7759–7770.
[13] K. Rajasekhar, N. Narayanaswamy, N.A. Murugan, K. Viccaro, H.G. Lee, K. Shah, T. Govindaraju, Abeta plaque-selective NIR fluorescence probe to differentiate Alzheimer's disease from tauopathies, Biosens. Bioelectron. 98 (2017) 54–61.
[14] M. Cui, Past and recent progress of molecular imaging probes for beta-amyloid plaques in the brain, Curr. Med. Chem. 21 (2014) 82–112.
[15] W. Yang, Y. Wong, O.T. Ng, L.P. Bai, D.W. Kwong, Y. Ke, Z.H. Jiang, H.W. Li, K. K. Yung, M.S. Wong, Inhibition of beta-amyloid peptide aggregation by multifunctional carbazole-based fluorophores, Angew Chem. Int. Ed. Engl. 51 (2012) 1804–1810.
[16] A. Kaur, A. Kaur, D. Goyal, B. Goyal, How does the mono-Triazole derivative modulate Abeta42 aggregation and disrupt a Protofibril structure: insights from molecular dynamics simulations, ACS Omega 5 (2020) 15606–15619.
[17] Y. Li, D. Xu, S.L. Ho, H.W. Li, R. Yang, M.S. Wong, A theranostic agent for in vivo near-infrared imaging of beta-amyloid species and inhibition of beta-amyloid aggregation, Biomaterials 94 (2016) 84–92.
[18] Y. Li, D. Xu, A. Sun, S.L. Ho, C.Y. Poon, H.N. Chan, O.T.W. Ng, K.K.L. Yung, H. Yan, H.W. Li, M.S. Wong, Fluoro-substituted cyanine for reliable in vivo labelling of amyloid-beta oligomers and neuroprotection against amyloid-beta induced toxicity, Chem. Sci. 8 (2017) 8279–8284.
[19] Y. Li, C. Chen, D. Xu, C.Y. Poon, S.L. Ho, R. Zheng, Q. Liu, G. Song, H.W. Li, M. S. Wong, Effective theranostic cyanine for imaging of amyloid species in vivo and cognitive improvements in mouse model, ACS Omega 3 (2018) 6812–6819.
[20] H. Oakley, S.L. Cole, S. Logan, E. Maus, P. Shao, J. Craft, A. Guillozet-Bongaarts, M. Ohno, J. Disterhoft, L. Van Eldik, R. Berry, R. Vassar, Intraneuronal beta-amyloid aggregates, neurodegeneration, and neuron loss in transgenic mice with five familial Alzheimer's disease mutations: potential factors in amyloid plaque formation, J. Neurosci. 26 (2006) 10129–10140.
[21] R. Belfiore, A. Rodin, E. Ferreira, R. Velazquez, C. Branca, A. Caccamo, S. Oddo, Temporal and regional progression of Alzheimer's disease-like pathology in 3xTg-AD mice, Aging Cell 18 (2019), e12873.
[22] A. Iyaswamy, S.K. Krishnamoorthi, J.X. Song, C.B. Yang, V. Kaliyamoorthy, H. Zhang, S.G. Sreenivasmurthy, S. Malampati, Z.Y. Wang, Z. Zhu, B.C. Tong, K. H. Cheung, J.H. Lu, S.S.K. Durairajan, M. Li, NeuroDefend, a novel Chinese medicine, attenuates amyloid-beta and tau pathology in experimental Alzheimer's disease models, J. Food Drug Anal. 28 (2020) 132–146.
[23] J.X. Song, S. Malampati, Y. Zeng, S.S.K. Durairajan, C.B. Yang, B.C. Tong, A. Iyaswamy, W.B. Shang, S.G. Sreenivasmurthy, Z. Zhu, K.H. Cheung, J.H. Lu, C. Tang, N. Xu, M. Li, A small molecule transcription factor EB activator ameliorates beta-amyloid precursor protein and Tau pathology in Alzheimer's disease models, Aging Cell 19 (2020), e13069.
[24] A. Iyaswamy, S.K. Krishnamoorthi, Y.W. Liu, J.X. Song, A.K. Kammala, S. G. Sreenivasmurthy, S. Malampati, B.C.K. Tong, K. Selvarasu, K.H. Cheung, J. H. Lu, J.Q. Tan, C.Y. Huang, S.S.K. Durairajan, M. Li, Yuan-Hu, Zhi Tong, Prescription mitigates tau pathology and alleviates memory deficiency in the preclinical models of Alzheimer's disease, Front. Pharmacol. 11 (2020) 584770.
[25] A. Iyaswamy, S.K. Krishnamoorthi, H. Zhang, S.G. Sreenivasmurthy, Z. Zhu, J. Liu, C.F. Su, X.J. Guan, Z.Y. Wang, K.H. Cheung, J.X. Song, S.S.K. Durairajan, M. Li, Qingyangshen mitigates amyloid-beta and Tau aggregate defects involving PPARalpha-TFEB activation in transgenic mice of Alzheimer's disease, Phytomedicine 91 (2021) 153648.
[26] S.G. Sreenivasmurthy, A. Iyaswamy, S. Krishnamoorthi, S. Senapati, S. Malampati, Z. Zhu, C.F. Su, J. Liu, X.J. Guan, B.C. Tong, K.H. Cheung, J.Q. Tan, J.H. Lu, S.S. K. Durairajan, J.X. Song, M. Li, Protopine promotes the proteasomal degradation of pathological tau in Alzheimer's disease models via HDAC6 inhibition, Phytomedicine 96 (2022) 153887.
[27] A.R. Ladiwala, J. Litt, R.S. Kane, D.S. Aucoin, S.O. Smith, S. Ranjan, J. Davis, W. E. Van Nostrand, P.M. Tessier, Conformational differences between two amyloid beta oligomers of similar size and dissimilar toxicity, J. Biol. Chem. 287 (2012) 24765–24773.
[28] M. Stefani, Structural features and cytotoxicity of amyloid oligomers: implications in Alzheimer's disease and other diseases with amyloid deposits, Prog. Neurobiol. 99 (2012) 226–245.
[29] R. Ismail, P. Parbo, L.S. Madsen, A.K. Hansen, K.V. Hansen, J.L. Schaldemose, P. L. Kjeldsen, M.G. Stokholm, H. Gottrup, S.F. Eskildsen, D.J. Brooks, The relationships between neuroinflammation, beta-amyloid and tau deposition in Alzheimer's disease: a longitudinal PET study, J. Neuroinflammation 17 (2020) 151.
[30] Y. Li, Z. Sun, Q. Cao, M. Chen, H. Luo, X. Lin, F. Xiao, Role of amyloid beta protein receptors in mediating synaptic plasticity, Biomed Rep. 6 (2017) 379–386.
[31] B. Styr, I. Slutsky, Imbalance between firing homeostasis and synaptic plasticity drives early-phase Alzheimer's disease, Nat. Neurosci. 21 (2018) 463–473.
[32] G.F. Chen, T.H. Xu, Y. Yan, Y.R. Zhou, Y. Jiang, K. Melcher, H.E. Xu, Amyloid beta: structure, biology and structure-based therapeutic development, Acta Pharmacol. Sin. 38 (2017) 1205–1235.
[33] T. Zhang, D. Chen, T.H. Lee, Phosphorylation signaling in APP processing in Alzheimer's disease, Int. J. Mol. Sci. 21 (2019).
[34] R.A. Nixon, D.S. Yang, Autophagy failure in Alzheimer's disease–locating the primary defect, Neurobiol. Dis. 43 (2011) 38–45.
[35] R. Puertollano, S.M. Ferguson, J. Brugarolas, A. Ballabio, The complex relationship between TFEB transcription factor phosphorylation and subcellular localization, EMBO J. 37 (2018).
[36] C. Settembre, C. Di Malta, V.A. Polito, M. Garcia Arencibia, F. Vetrini, S. Erdin, S. U. Erdin, T. Huynh, D. Medina, P. Colella, M. Sardiello, D.C. Rubinsztein, A. Ballabio, TFEB links autophagy to lysosomal biogenesis, Science 332 (2011) 1429–1433.
[37] J.X. Song, J. Liu, Y. Jiang, Z.Y. Wang, M. Li, Transcription factor EB: an emerging drug target for neurodegenerative disorders, Drug Discov. Today (2020).
[38] Y. Hong-Qi, S. Zhi-Kun, C. Sheng-Di, Current advances in the treatment of Alzheimer's disease: focused on considerations targeting Abeta and tau, Transl. Neurodegener. 1 (2012) 21.
[39] Q. Xiao, P. Yan, X. Ma, H. Liu, R. Perez, A. Zhu, E. Gonzales, D.L. Tripoli, L. Czerniewski, A. Ballabio, J.R. Cirrito, A. Diwan, J.M. Lee, Neuronal-targeted TFEB accelerates lysosomal degradation of APP, reducing abeta generation and amyloid plaque pathogenesis, J. Neurosci. 35 (2015) 12137–12151.